CENTER FOR CONNECTED AND AUTOMATED TRANSPORTATION

Final Report #ICT-21-038
November 2021

Truck-Platooning Impacts on Flexible Pavements: Experimental and Mechanistic Approaches

Imad L. Al-Qadi
Bliss Professor of Engineering

Hasan Ozer
Associate Professor

Egemen Okte
Research Assistant

Ashraf Alrajhi
Graduate Student

Aravind Ramakrishnan
Master's Student

ILLINOIS CENTER FOR TRANSPORTATION

DISCLAIMER

Funding for this research was provided by the Center for Connected and Automated Transportation under Grant No. 69A3551747105 of the U.S. Department of Transportation, Office of the Assistant Secretary for Research and Technology (OST-R), University Transportation Centers Program. The contents of this report reflect the views of the authors, who are responsible for the facts and the accuracy of the information presented herein. This document is disseminated under the sponsorship of the Department of Transportation, University Transportation Centers Program, in the interest of information exchange. The U.S. Government assumes no liability for the contents or use thereof.

Suggested APA Format Citation:

Ramakrishnan, A., Alrajhi, A., Okte, E., Ozer, H., & Al-Qadi, I.L. (2021). *Truck-platooning impacts on flexible pavements: Experimental and mechanistic approaches* (Report No. ICT-21-038). Illinois Center for Transportation. https://doi.org/10.36501/0197-9191/21-038

Contacts

For more information:

Aravind Ramakrishnan
University of Illinois at Urbana–Champaign
B235 Newmark Civil Engineering Laboratory
205 North Mathews Avenue, Urbana, IL 61801
aravind4@illinois.edu
https://ict.illinois.edu

CCAT
University of Michigan Transportation Research Institute
2901 Baxter Road
Ann Arbor, MI 48152
uumtri-ccat@umich.edu
(734) 763-2498
www.ccat.umtri.umich.edu

TECHNICAL REPORT DOCUMENTATION PAGE

1. Report No.	2. Government Accession No.	3. Recipient's Catalog No.
ICT-21-038	N/A	N/A

4. Title and Subtitle	5. Report Date
Truck-Platooning Impacts on Flexible Pavements: Experimental and Mechanistic Approaches	November 2021
	6. Performing Organization Code N/A

7. Author(s)	8. Performing Organization Report No.
Aravind Ramakrishnan, Ashraf Alrajhi, Egemen Okte, Hasan Ozer, and Imad L. Al-Qadi	ICT-21-038 UILU-ENG-2021-2038

9. Performing Organization Name and Address	10. Work Unit No.
Illinois Center for Transportation Department of Civil and Environmental Engineering University of Illinois at Urbana–Champaign 205 North Mathews Avenue, MC-250 Urbana, IL 61801	N/A
	11. Contract or Grant No. Grant No. 69A3551747105

12. Sponsoring Agency Name and Address	13. Type of Report and Period Covered
Center for Connected and Automated Transportation University of Michigan Transportation Research Institute 2901 Baxter Road Ann Arbor, MI 48152	Final Report
	14. Sponsoring Agency Code

15. Supplementary Notes

Funding under Grant No. 69A3551747105 U.S. Department of Transportation, Office of the Assistant Secretary for Research and Technology (OST-R), University Transportation Centers Program.
https://doi.org/10.36501/0197-9191/21-038

16. Abstract

Truck platoons are expected to improve safety and reduce fuel consumption. However, their use is projected to accelerate pavement damage due to channelized-load application (lack of wander) and potentially reduced duration between truck-loading applications (reduced rest period). The effect of wander on pavement damage is well documented, while relatively few studies are available on the effect of rest period on pavement permanent deformation. Therefore, the main objective of this study was to quantify the impact of rest period theoretically, using a numerical method, and experimentally, using laboratory testing. A 3-D finite-element (FE) pavement model was developed and run to quantify the effect of rest period. Strain recovery and accumulation were predicted by fitting Gaussian mixture models to the strain values computed from the FE model. The effect of rest period was found to be insignificant for truck spacing greater than 10 ft. An experimental program was conducted, and several asphalt concrete (AC) mixes were considered at various stress levels, temperatures, and rest periods. Test results showed that AC deformation increased with rest period, irrespective of AC-mix type, stress level, and/or temperature. This observation was attributed to a well-documented hardening–relaxation mechanism, which occurs during AC plastic deformation. Hence, experimental and FE-model results are conflicting due to modeling AC as a viscoelastic and the difference in the loading mechanism. A shift model was developed by extending the time–temperature superposition concept to incorporate rest period, using the experimental data. The shift factors were used to compute the equivalent number of cycles for various platoon scenarios (truck spacings or rest period). The shift model was implemented in AASHTOware pavement mechanic–empirical design (PMED) guidelines for the calculation of rutting using equivalent number of cycles.

17. Key Words	18. Distribution Statement
Truck Platooning, Platoons, Resting Period, Hardening-Relaxation, Pavement Damage, Shift Model, repeated load, permanent deformation	No restrictions. This document is available through the National Technical Information Service, Springfield, VA 22161.

19. Security Classif. (of this report)	20. Security Classif. (of this page)	21. No. of Pages	22. Price
Unclassified	Unclassified	44	N/A

ACKNOWLEDGMENT, DISCLAIMER, MANUFACTURERS' NAMES

This project was conducted in cooperation with the Center for Connected and Automated Transportation and the Illinois Center for Transportation. The contents of this report reflect the view of the authors, who are responsible for the facts and the accuracy of the data presented herein. The contents do not necessarily reflect the official views or policies of CCAT or ICT. This report does not constitute a standard, specification, or regulation. Trademark or manufacturers' names appear in this report only because they are considered essential to the object of this document and do not constitute an endorsement of the product by CCAT or ICT.

TABLE OF CONTENTS

LIST OF FIGURES

LIST OF TABLES

CHAPTER 1: INTRODUCTION

Despite the potential numerous advantages of truck platooning enabled by connectivity and possible automated driving systems, there are concerns regarding its impact on pavement performance due to expected channelized traffic and reduced spacing between trucks within the platoon (Fagnant and Kockelman, 2015; Liang et al., 2016; Gungor and Al-Qadi, 2020a). The temporal and spatial shifts in truck movements were expected to affect the pavement-deterioration progress (Birgisson et al., 2020; Gungor and Al-Qadi, 2020a). Reduced rest period and lack of wander between trucks within the platoon were reported to increase pavement rutting and fatigue-damage accumulation (Gungor and Al-Qadi, 2020b). Various lateral and spatial truck positions in a platoon may impact pavement's response differently (Figure 1). In this study, an experimental program supported by mechanistic numerical models was developed and performed to translate truck-platoon configurations to evaluate the impact of rest period on permanent deformation of pavement.

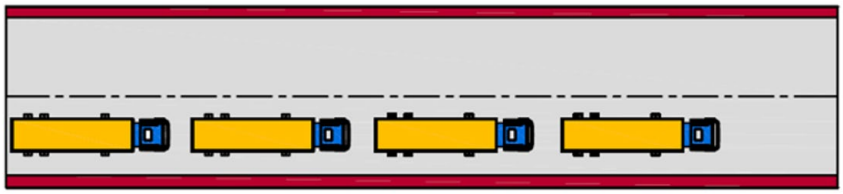

A. S1: Platoons

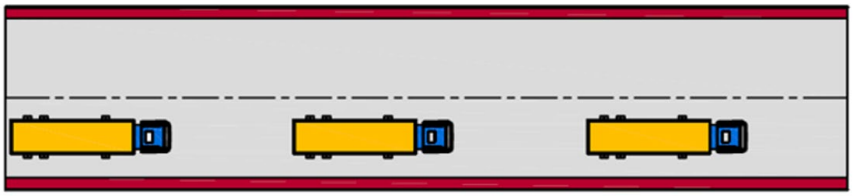

B. S2: Neither platoons nor wander

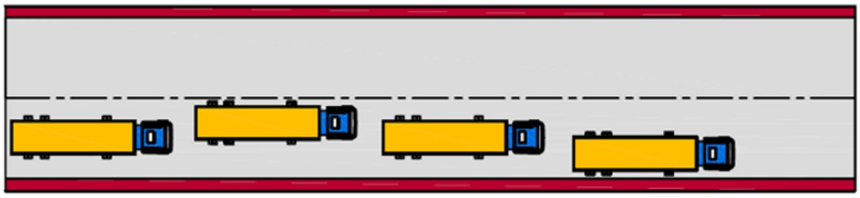

C. S3: Wander with platoons

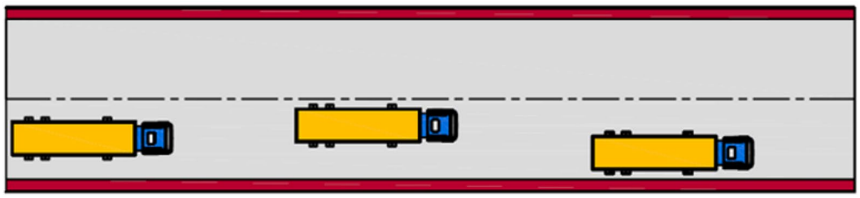

D. S4: Wander with no platoons

Figure 1. Illustrations. Different scenarios of platoon configurations.
Source: Gungor and Al-Qadi, 2020a

Because truck-platoon technology has been recently developed and is not commonly applied, its impact on pavement performance has not been assessed in the field. Driverless trucks were used in the WesTrack project in the 2000s to test various pavement structures and asphalt concrete (AC) mixture designs (Epps et. al, 2002). The premature failure of some sections was attributed to channelized loading (Epps et. al, 2002). Gungor and Al-Qadi (2020b) introduced the effect of lateral position to the mechanistic–empirical pavement-design guide (MEPDG) damage-prediction equations. It was observed that permanent deformation increased when wander was absent. Noorvand et al. (2017) investigated the impact of the positioning of truck loadings on the long-term performance of transportation infrastructure, by simulating different scenarios utilizing MEPDG. The highest damage was predicted with zero wander; a single climatic location, pavement type, and traffic combination were used (Noorvand et al., 2017).

Rest period governed by the distance between trucks can have a significant impact on AC pavement performance due to the viscoelastic nature of the AC materials. The effect of rest period on the AC cracking potential is well documented in the literature (Kim et al., 2001; Daniel and Kim, 2001; Kim and Roque, 2006; Underwood and Zeiada, 2014). Increasing the rest period was shown to allow for increasing strain recovery and healing time, especially at the onset of damage progression. However, the relationship between rest period and permanent deformation is relatively less studied. Kim and Kim (2017) reported an insignificant effect of rest periods on permanent deformation when using an optimal pulse configuration during a repeated load-deformation experiment. This behavior could be attributed to the relatively high rest-period values. In contrast, Darabi et al. (2013) developed nonlinear constitutive relationships, based on viscoelasticity and viscoplasticity theories, to evaluate the effect of rest period. The overall response of AC mixes to cyclic loading with varying pulse configuration was explained by a hardening–relaxation mechanism incorporated into the constitutive relationship. Although a limited number of parameters and experiments was considered, including a rest period between loading pulses resulted in higher permanent deformations due to hardening–relaxation.

Similar to temperature, stress magnitude, and material's permanent-deformation resistance, pulse configuration and rest periods could be important. However, the degree of significance is related to the AC's inherent characteristics (e.g., binder properties; aggregate size, gradation, and packing; and AC air void), which influence the AC strain recovery and hardening–relaxation properties. Hence, rest period should be considered in pavement design when subjected to platoon loadings. To achieve that, there is a need to verify and quantify the impact of rest period on AC permanent deformation, considering a range of parameters representative of loading conditions in the field.

OBJECTIVE AND SCOPE

The main goal of this study is to characterize the impact of rest period on permanent-deformation resistance of AC pavements. Understanding the fundamental characteristics of the rest-period impact on permanent deformations would help develop optimized truck-platoon scenarios, considering pavement damage as one of the variables. The work presented in the report is an outcome of collaborative research conducted by the University of Illinois at Urbana–Champaign and Arizona State University as part the Center for Connected and Automated Vehicles, sponsored by the United States

Department of Transportation's (USDOT's) University Transportation Center at the University of Michigan. The goal of the collaborative research project was to develop permanent-deformation prediction models that consider rest period and could be integrated into mechanistic design approaches.

Research scope included experimental characterization of permanent deformations with varying rest periods and mechanistic modeling to incorporate the outcome into the AASHTO PMED. Specific research objectives were as follows:

- Characterize the extent of AC linear viscoelastic recovery and its impact on total AC deformation under various axle-loading configurations that represent platoons.
- Develop simplified models to describe the effect of rest period on AC permanent deformation that can be incorporated into mechanistic–empirical pavement-design platforms.
- Characterize experimentally the mechanisms of the rest-period effect on AC permanent deformation.
- Quantify the effect of temperature and stress level on rest period and its corresponding impact on AC permanent deformation.
- Determine the effect of rest-period duration on AC permanent deformation.

CHAPTER 2: BACKGROUND

The main benefit of driving trucks at a close distance from one another is reducing overall aerodynamic drag. Most of the aerodynamic drag, approximately 70% to 90%, is caused by the pressure difference, known as the pressure drag, between the front and rear of a truck, also referred to as the high- and low-pressure zones, respectively (Gaudet, 2014). In a platoon, the pressure drag on trailing trucks decreases because the truck in front blocks the air and lowers the pressure in the frontal zone. For a leading truck, the aerodynamic drag decreases because the trailing truck compresses the turbulent flow that increases the pressure in the low-pressure zone. Consequently, this reduction in aerodynamic drag leads to increased fuel efficiency. The effect on fuel consumption was documented in the literature review and discussed elsewhere (Al-Qadi et al., 2021).

With the introduction of platoons, the resting period—the period between two consecutive loads—is expected to decrease significantly. The impact of a reduced rest period on AC performance may be grouped into two categories: fatigue and rutting. Rest period on concrete pavement will mainly affect granular base erosion. In this chapter, a summary of the literature to describe the effect of rest period on AC is discussed.

Generally, AASHTOWare PMED is used to obtain the pavement responses (stresses and strains). Later, the pavement responses are used in transfer functions to compute distresses such as fatigue cracking and rutting. A pavement section is selected if computed distresses meet the failure criteria. An increasing number of state agencies in the United States use the above method to design flexible-pavement sections. There are several shortcomings of AASHTOWare PMED: (a) Linear elasticity is assumed for all layers in the pavement; (b) constant static loading is applied; and (c) layer interactions are modelled as simplified distributed springs. To overcome the above drawbacks, pavements were modelled using finite elements by Al-Qadi and coworkers (Al-Qadi and Yoo, 2007; Elseifi et al., 2006; Hernandez et al., 2016; Yoo and Al-Qadi, 2007; and Yoo et al., 2006).

IMPACT OF REST PERIOD ON MECHANISTIC RESPONSE OF VISCOELASTIC PAVEMENT

To investigate the impact of rest period on AC pavement responses, 204 finite-element (FE) simulations were conducted using ABAQUS. The simulation matrix is presented in Table 1. The weak and strong AC layer properties are extracted by conducting a statistical analysis of the Long-Term Pavement Performance (LTPP) dynamic modulus database (Hernandez et al., 2016). The objective of the simulations was to capture the time dependent of AC responses and observe their evolution prior to and after tire loading.

Table 1. Simulation Matrix for Single and Tandem Axles (from Al-Qadi et al., 2021)

Type	**Single Axle**	**Tandem Axle**
AC Layer Type	Strong and Weak	Strong and Weak
Structure	Thick (11-in AC, 70 mph) and Thin (4-in AC, 40 mph)	Thick (11-in, 70 mph) and Thin (4-in AC, 40 mph)
Tire Type	DTA, WBT, and Steering	DTA and WBT
Temperature	122°F, 68°F, and 18°F profiles	122°F, 68°F, and 18°F profiles
Half-Axle Load (kips)	6.75, 9, 11.25, 13.5, and 15.75	16.875
Total Number of Cases	**2×2×3×3×5 = 180 cases**	**2×2×2×3 = 24 cases**

* DTA: dual-tire assembly; WBT: wide-base tire.

Because tensile strains at the bottom of the AC layer are thought to be correlated to fatigue cracking in the field, transverse and longitudinal tensile strains at the bottom of the AC layer were obtained. Similarly, for rutting, maximum compressive strains in the AC and base and top of the subgrade were calculated. Critical tensile and compressive strains were collected during tire passage.

A truck platoon results in a reduced rest period between truck-load applications. Therefore, recovery of critical responses was extracted from the FE simulations. The recovery of tensile and compressive strains for two critical sections is presented in Figure 2. Because the time steps of the simulations were limited, the tail of the recovery end was not captured by the simulation. To mitigate this issue, Gaussian mixture models were used to fit the data to the tail end of the recovery curve. It was observed that critical responses recover fully after 0.1 sec. If two trucks are travelling 10 ft apart at 70 mph, the time it takes between the last tandem-axle loading of the first truck and the steering-axle of the second truck is approximately 0.1 sec. Therefore, it was concluded that the impact of rest period on viscoelastic AC pavement responses was insignificant for truck spacings larger than 10 ft.

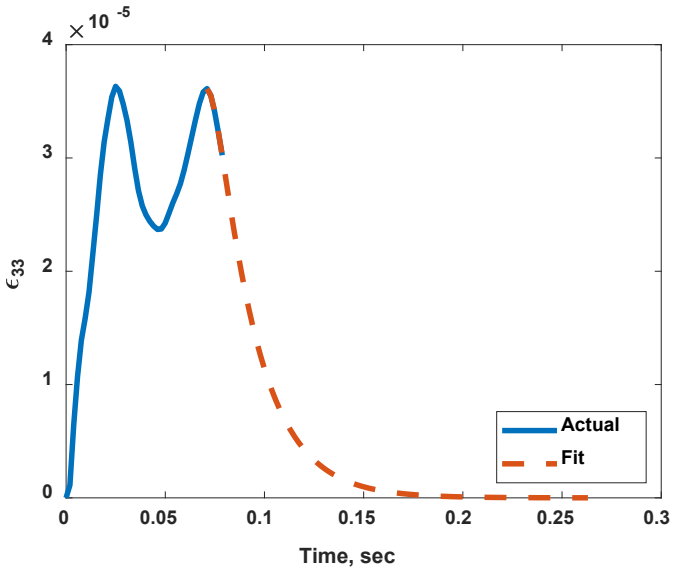

A. Tensile-Strain Response

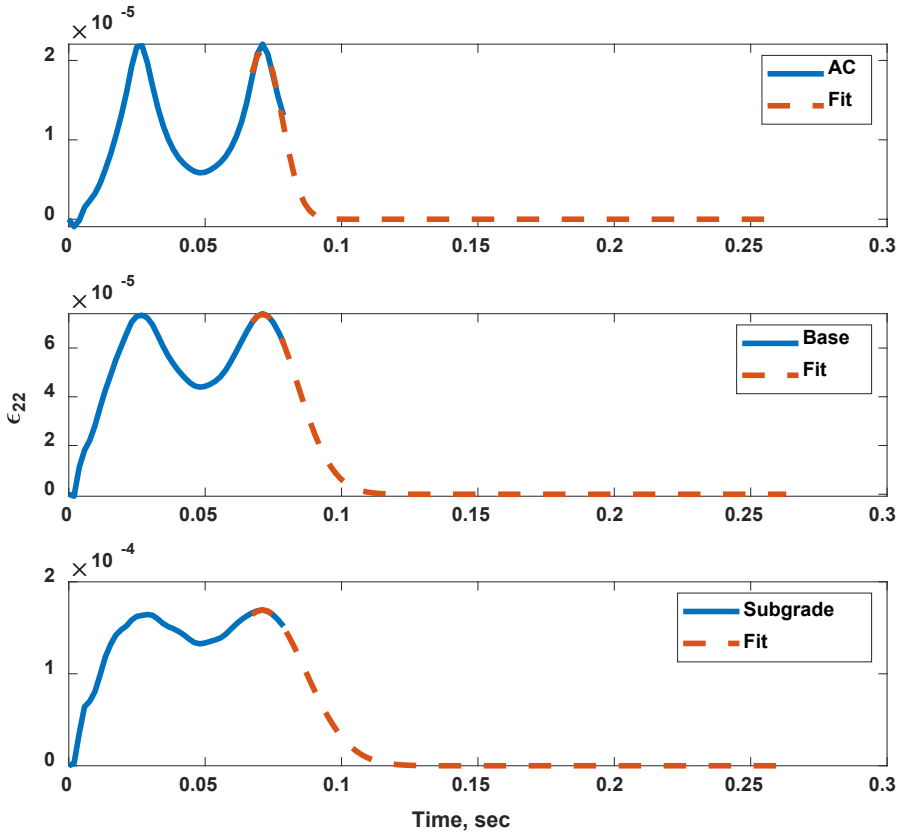

B. Compressive-Strain Response

Figure 2. Plots. Percentage of transverse-strain recovery.

Source: Al-Qadi et al., 2021

IMPACT OF REST PERIOD ON FLEXIBLE-PAVEMENT FATIGUE PROGRESSION

Properly designed and mixed AC has a self-healing capability of recovering microcracks when the pavement is not loaded (Kim and Little, 1989; Kim and Little, 1994). Introducing a rest period between two consecutive loads is expected to increase AC's service life. Self-healing occurs simultaneously with viscoelastic relaxation of AC, which also affects its fatigue life. Thus, it is important to separate the effects of viscoelastic relaxation from microcrack healing. A few key examples from the literature are discussed.

Daniel and Kim (2001) used the third-point flexure-fatigue (TFFT) test for studying the healing characteristics of AC mixes under three damage levels—low, medium, and high—and two temperatures—68° and 140°F. The results from a series of experiments showed that rest period increased the number of repetitions to failure. Results suggested that rest period increased AC elastic modulus, and healing occurred faster at higher temperatures (Figure 3). Additionally, healing characteristics are AC mix-dependent.

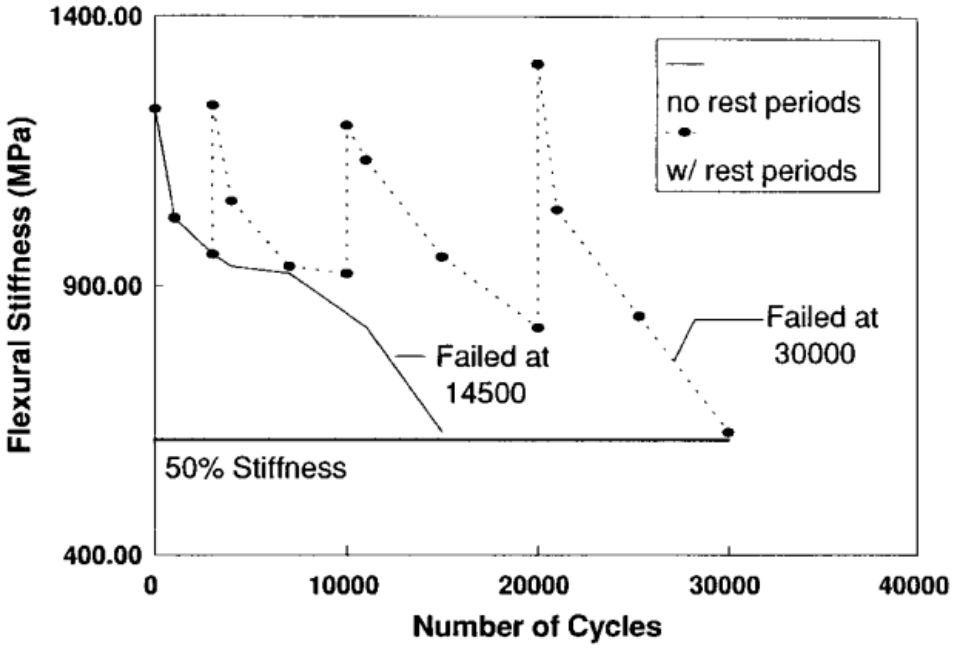

Figure 3. Graph. Flexural stiffness versus number of cycles (1 MPa = 145 psi).

Source: Daniel and Kim, 2001

Carpenter and Shen (2006) introduced a specifically designed fatigue-healing test to study AC-fatigue life and self-healing. The test was a modified version of a four-point flexural test with intermittently applied haversine loading. The polymer-modified AC mixes exhibited a faster healing rate, as compared to AC mixes with neat binder. A follow-up study conducted by Beranek and Carpenter (2009) introduced a transfer function (Figure 4), based on both laboratory and field tests, that explicitly uses rest period as input to determine the number of repetitions to failure.

$$N_f = 9500.6\,(RP + 1) + 6146.7$$

Figure 4. Equation. Calculation of the number of cycles to failure.

where N_f is the number of repetitions to failure and RP is the rest period (sec).

EFFECT OF REST PERIOD ON AC RUTTING

When AC is loaded and unloaded, the resultant strain has four components: elastic, viscoelastic, plastic, and viscoplastic. *Elastic strain* refers to strain that is immediately recovered when load is removed. *Plastic strain* is unrecoverable and immediately occurs when a load is applied. *Viscoelastic and viscoplastic strains* are time-dependent. Viscoelastic strains are recoverable, while viscoplastic strains are unrecoverable (Figure 5). The permanent strain, such as normalized rutting, is a summation of the plastic, viscoelastic, and viscoplastic strains. Thus, the permanent strain has two components that are time-dependent; and it is affected by both rest period and loading time.

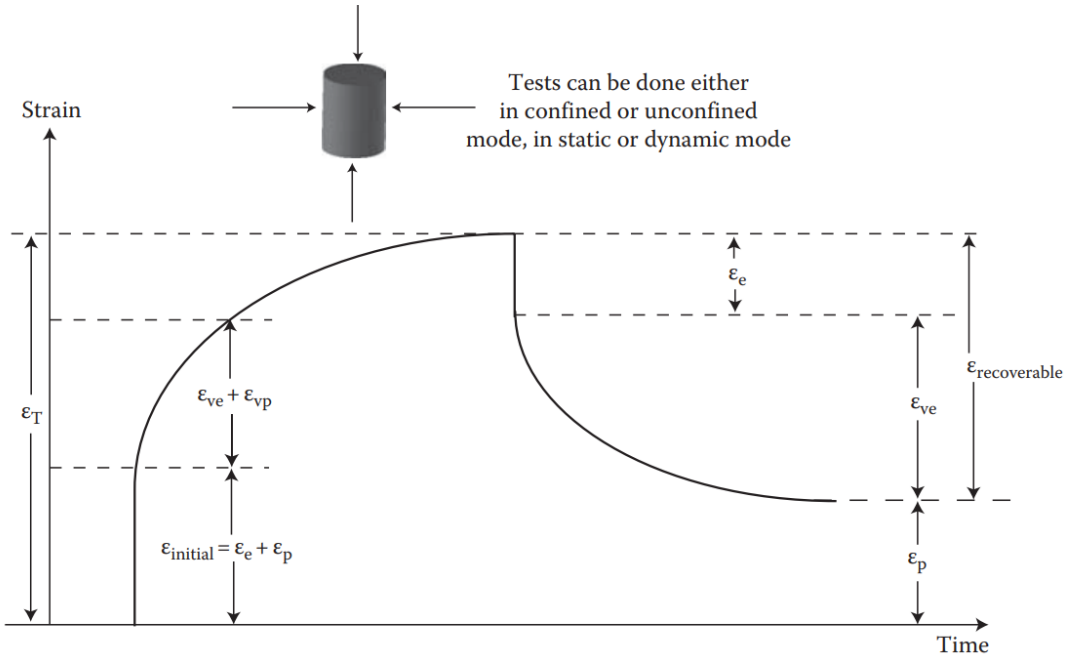

Figure 5. Graph. Components of strain in a creep testing.

Source: Mallick and Tahar, 2013

Temperature, stress level, loading rate, and AC-mixture characteristics affect AC permanent deformation. The AC permanent deformation is typically characterized using repeated-load permanent-deformation (RLPD) tests, such as AASHTO T378 flow number and flow time. The experiment is conducted at a selected stress level and temperature, representing the region of application. Uniaxial deviatoric stresses are applied at a fixed haversine pulse configuration with 0.1-sec loading time. The flow-number experiments are commonly used to evaluate the AC-mix permanent deformation and the impact of factors such as reclaimed asphalt pavement (RAP), mix type, and binder modification (Witzcak and Ed, 2002). The Francken model, a phenomenological permanent-deformation prediction model presented in Figure 6, was developed by Biligiri et al. (2007). The model represents primary and secondary regions, using a power function; and a tertiary region, using an exponential model. The flow-number value at which the tertiary flow starts can be derived mathematically using the Francken model, as presented in Figure 6 and 7 (Biligiri et al., 2007 and Witczak, 2007).

$$\varepsilon_p = AN^B + C(e^{DN} - 1)$$

Figure 6. Equation. The Francken model.

where Ɛp = permanent deformation or plastic strain; N = number of loading cycles; and A, B, C, and D = regression constants and are a function of the AC-mix quality, test temperature, and stress state used in the repeated-load study.

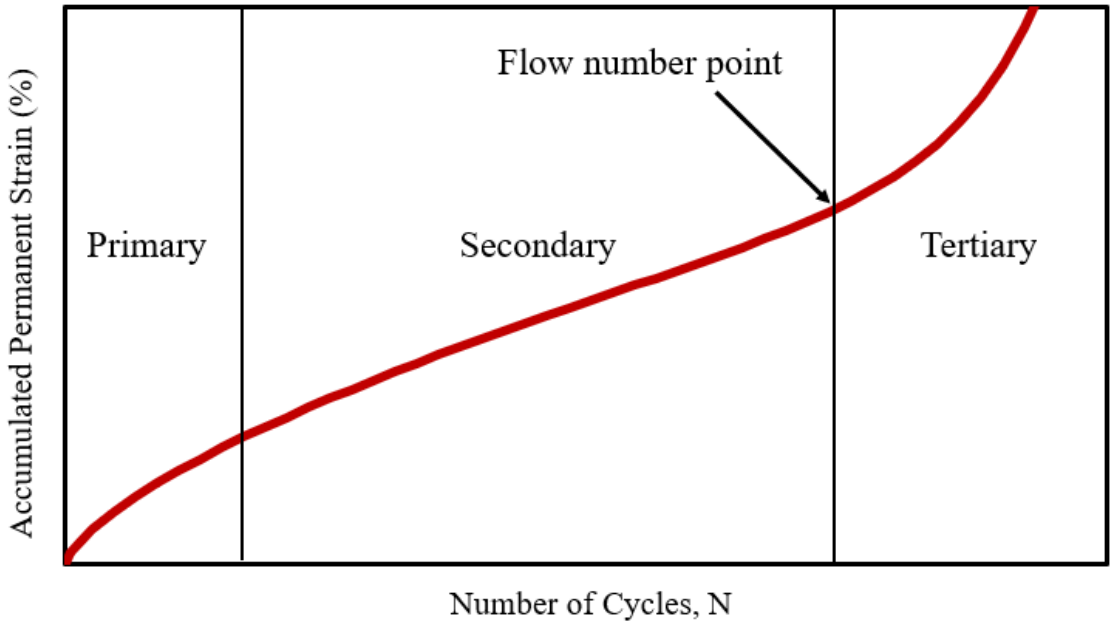

Figure 7. Graph. Relationship between permanent strain and the number of cycles in a flow-number test.

Source: Witczak, 2007

The effects of loading time and rest period were recognized as critical parameters primarily for fatigue characterization of AC mixtures (Kim et al., 2001; Kim et al., 2006; Daniel et al., 2001; Underwood and Zeiada, 2014). Few studies have focused on characterizing the impact of pulse configurations on permanent deformations. Qi and Witzcak (1998) showed the effect of loading time at constant rest periods and the rest periods at constant loading times. One dense-graded AC with a 1/2-in nominal maximum aggregate size (NMAS) was used in accordance with Maryland Department of Transportation (MDOT) specifications. All samples were tested using a repeated-cyclic creep test. Three loading times with square wave (0.1, 10, and 1,000 sec), three rest periods (0.9, 10, and 1,000 sec), two stress levels (10 and 20 psi), and two temperatures (100° and 130°F) were applied. It was shown that the permanent deformation increased with increasing loading time at constant rest periods and decreased with increasing rest periods at a constant loading time (Qi and Witzcak, 1998).

Fundamental permanent-deformation models were also developed using viscoelasticity and viscoplasticity constitutive relationships (Darabi et al., 2012; Yun and Kim, 2011; Gibson et al., 2003; Chehab et al., 2003). Although plasticity-based characterization and models require advanced equipment and modeling techniques, such fundamental constitutive models allow more consistent evaluation of loading time and rest period. The viscoelastic and viscoplastic constitutive models were built on recognizing the limitations of the Perzyna viscoplastic model to capture cyclic hardening observed in the secondary region of permanent deformations (Darabi et al., 2012; Darabi et al., 2013; Yun and Kim, 2011). The effect of rest period was captured consistently with experiments by adding a relaxation property to the hardening behavior. Using the model feature touted as hardening–relaxation, or hardening–softening, it was demonstrated that as rest period increased, permanent

deformation also increased. As an example, the effect of rest period and model predictions is presented in Figure 8.

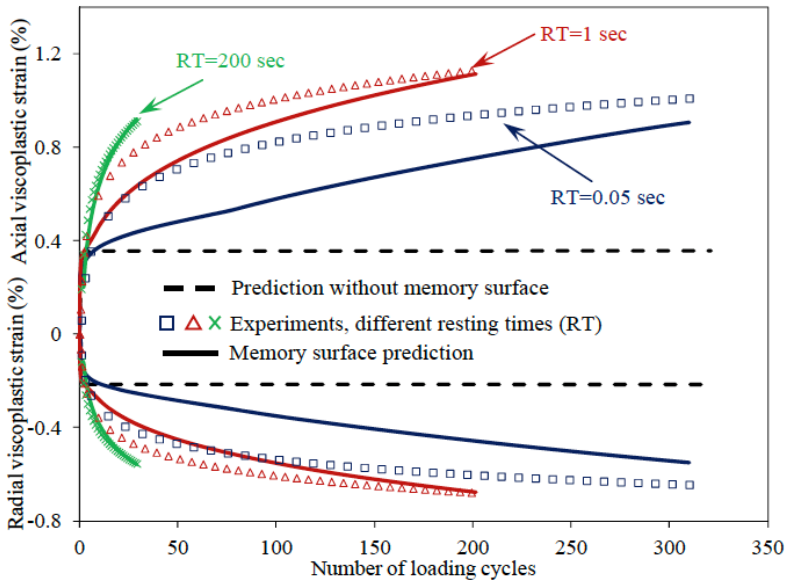

Figure 8. Graph. Effect of rest period on permanent deformation, using model predictions and experimental data.

Source: Darabi et al., 2012

The physical explanation of hardening–relaxation was described by the reorientation of aggregate structure from a hardened state to a more relaxed previous state less resistant to deformation. As more time was allowed between cycles, relaxation of aggregate structure continued to a state less resistant to deformation; hence, the more permanent deformation (Darabi et al., 2012; Darabi et al., 2013; Yun and Kim, 2011; Jahangiri et al., 2017). The hypothesis of aggregate reorientation with applied cycles is illustrated in Figure 9.

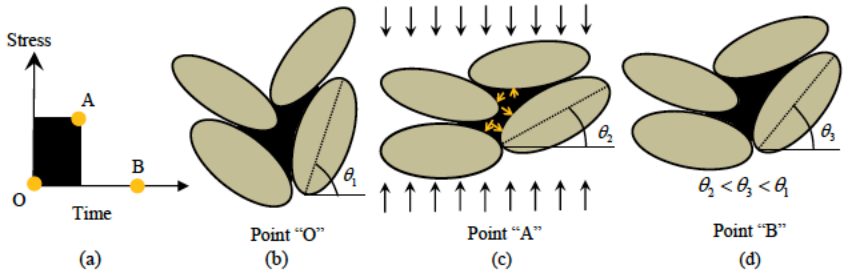

Figure 9. Illustration. Schematic representation of hardening–relaxation.

Source: Darabi et al., 2012

Yun and Kim (2011) implemented a model considering the viscoplastic rate-dependent hardening–softening behavior using Perzyna's flow rule and a rate-dependent yield-stress function. Some of

those experiments were also discussed in detail in Yun's doctoral dissertation (Yun, 2008). The repetitive creep and recovery test was conducted at a temperature of 131°F and high-confining pressure of 72.52 psi to reduce the effect of aggregate friction on viscoplastic strain. To calibrate and verify the development of the model, three scenarios of loading conditions were performed on the repetitive creep and recovery test as follows: (a) variable time (VT), (b) constant loading time (CLT), and (c) variable load (VL). The VT and CLT tests were used to capture the rate hardening and softening effects on viscoplastic strains, along with the effect of rest period. During the CLT experiments, the experiments with shorter pulse time resulted in higher viscoplastic strains. For example, viscoplastic strain after testing with a 0.4-sec pulse time was over 3%, whereas it was around 1.5% with a 1.6-sec pulse time. Because loading time was constant, as the pulse time reduces, a greater number of pulses can be applied. According to the authors, every loading and long unloading (rest period) sequence is an opportunity for the material to soften (or unlock from a hardened state). Longer rest periods (200 sec) were also compared to the tests comprised of pulses with 0.05-sec and 0.1-sec pulse periods. Smaller viscoplastic strains were observed as the rest period became shorter. The effect of rest period was compared to the effect of reducing deviatoric stress. It was concluded that rest period can have comparable impact on viscoplastic strains with the changes in the deviatoric stress levels and should not be ignored. Mechanisms of hardening and softening were explained and defined by viscoplastic constitutive relationships.

Darabi et al. (2013) enhanced the constitutive models to predict the viscoplastic response of AC under different cyclic-loading conditions and rest periods at a high temperature (i.e., 131°F). A viscoplastic hardening–relaxation memory surface was introduced to obtain an initiation and evolution criteria of the hardening–relaxation effect by memorizing the maximum-experienced viscoplastic strain during the loading history. Similar to the results presented by Yun and Kim, as rest period increased, permanent deformation increased (Yun and Kim, 2011). The developed constitutive model was implemented in ABAQUS, a commercial finite-element software program, using a material subroutine. Permanent-deformation predictions using the numerical simulations at high temperatures subjected to cyclic compression loading were consistent with the experimental data by using the hardening–relaxation model with the memory surface (Darabi et al., 2013).

The effect of recovered viscoelastic strains on viscoplastic behavior of AC was investigated by Jahangiri et al., 2017. They investigated the effect of different loading times and residual stress levels on the permanent deformation of 3/4-in NMAS dense-graded AC using repetitive cyclic loading. Tests were conducted at 86°F using 5-sec haversine loading and 6.4-sec trapezoidal loading to reflect high-volume traffic with low speed. Four rest periods (0, 5, 10, and 20 sec) were introduced to trapezoidal loading. One rest period (5 sec) was introduced to the haversine loading. The primary stress level (130.5 psi) was applied to the trapezoidal loading, while 108.8 psi was applied to the haversine loading. Three different residual stresses after unloading (87, 54.4, and 0 psi) were used for trapezoidal loading. Three different residual stresses (108.8, 87, and 65.27 psi) were applied for haversine loading. It was reported that when rest period increased, viscoplastic strain increased. Moreover, when residual stress increased, total strain decreased at constant rest periods.

Kim and Kim (2017) investigated the effect of rest period on permanent deformation by introducing three rest periods (3, 5, and 10 sec) and a constant loading time (0.4 sec at 129.2°F) by triaxial

repeated-load permanent-deformation tests. Variable stress levels were applied with reverse loading blocks at 70, 100, and 130 psi with 200 cycles in each block and a confining pressure of 10 psi. It was shown that the effect of rest period on permanent strain at a high temperature was insignificant due to the relatively high rest-period values (Kim and Kim, 2017).

Motevalizadeh et al. (2018) developed a regression model for predicting permanent deformation by conducting a series of 36 RLPD tests: two rest periods, two temperatures, three loading times, and three levels of stress. The developed regression equation is presented in Figure 10. . Furthermore, temperature was found to be the critical parameter for AC permanent-deformation behavior.

$$\varepsilon = a N^{b}$$

$$\alpha = 0.6768\ T^{-1.4968} S^{0.2834} L^{0.1788} R^{0.5692}$$

$$b = -2.2616 - 0.3256\ log(S) + 0.033\ log(L) - 0.1274\ log(R) + 1.1036\ log(T)$$

Figure 10. Equation. Regression model for permanent deformation

The coefficients of the strain model (a, b) are functions of rest period, temperature, loading time, and stress level. To understand the effect of rest period, synthetic curves were generated by keeping other variables constant, as presented in Figure 11. It can be observed that permanent deformation increases with the rest period. The trends are similar to what was observed in the experimental program conducted for this study.

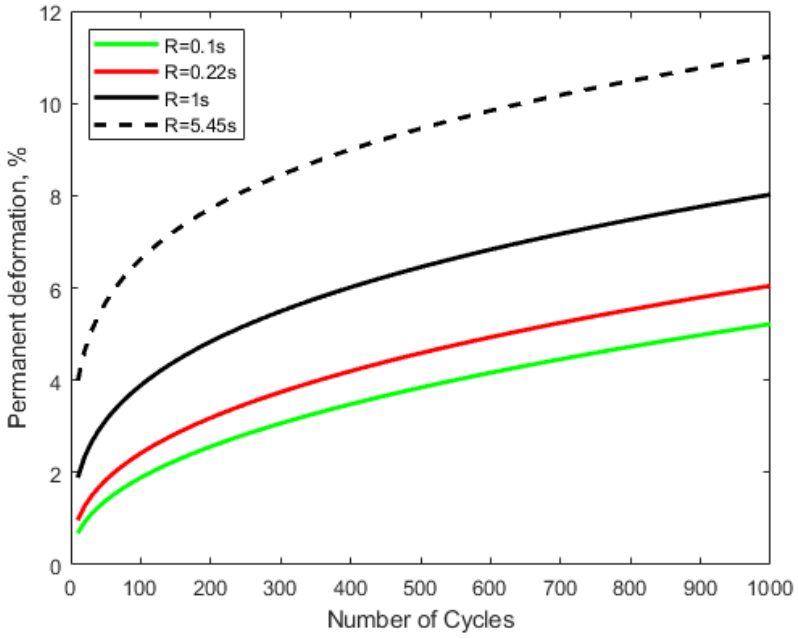

Figure 11. Illustration. Permanent deformation versus number of cycles for different rest periods.

In the same study, Motevalizadeh et al. (2018) presented a secondary regression equation with additional constant value for coefficient 'a.' The influence of parameters was completely changed, as shown in the Figure 12. .

$$\epsilon = aN^b$$

$$a = -0.1207 + 0.0957\, T^{0.1593} S^{-0.0495} L^{0.000291} R^{0.1647}$$

$$b = -1.3416 + 0.3532log(S) + 0.4401log(L) + 0.0842log(R) - 0.1522log(T)$$

Figure 12. Equation. Second regression model for permanent deformation.

Similar to Figure 11., curves were generated to understand the influence of rest period (other variables were assumed constant) using the equations in Figure 12. The curves are shown Figure 13. Though the trends are similar to Figure 11., the extent of influence of the rest period is completely different. Varying trend is one of the drawbacks of using a regression approach, as the influence of parameters could be significantly different based on the equation chosen to fit the experimental data. Regression would be a better approach if experimental data collected were large enough to produce almost similar trends and influence of the parameters.

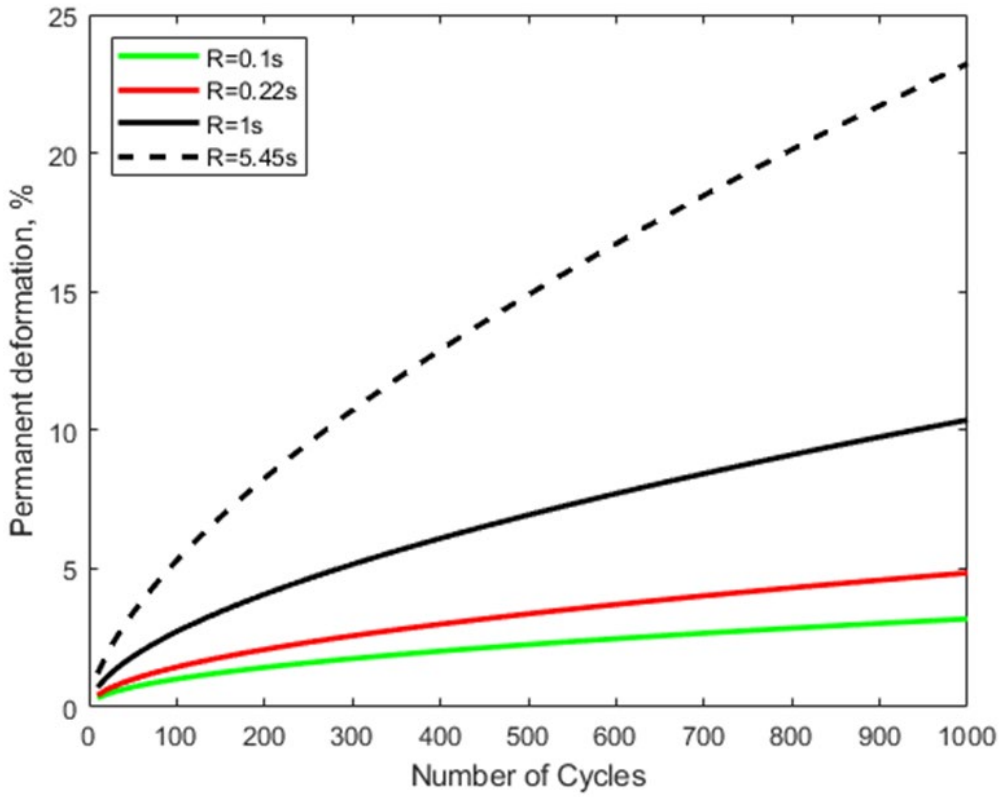

Figure 13. Illustration. Permanent deformation versus number of cycles for different rest periods, using secondary regression equation.

Because the hypothesis behind the hardening–softening, or hardening–relaxation, theory hinges upon aggregate structure and reorientation during cyclic loading, it is crucial to test this assumption with similar experiments on granular materials. Alnedawi et al. (2019) explored the effect of rest period on the deformation behavior of two types of crushed granular materials (i.e., basalt and granite), using repeated-load triaxial tests and finite-element (FE) modeling using the Drucker-Prager model. The tests were conducted in two phases. Initially, a trapezoidal pulse for 1 sec of loading time and 2 sec of rest period was applied with three deviatoric stresses of 50.8, 65.3, and 79.8 psi as a block within one test at a confining pressure of 7.25 psi. The number of cycles for each stress block was 10,000. Then a trapezoidal pulse for 3 sec of loading time and no rest period was applied with the same parameters as the first phase. It was concluded that rest period had a significant effect on the permanent deformations. The plasticity model used in the FE simulations resulted in higher errors in prediction for the cases with a rest period, as compared to those without a rest period. The study found that the rest-period impact could be due to the hardening–relaxation, or hardening–softening, phenomenon.

SUMMARY

As opposed to the positive effect of increasing rest periods on AC fatigue cracking due to the healing and recovery of strains, rest period was shown in some studies to have an opposite impact on AC permanent deformation. According to the hypothesis used in the developed plasticity-based constitutive model, aggregate structure and its reorientation change during load pulses with varying rest periods, which affects AC permanent-deformation resistance. The hardening–relaxation, or hardening–softening, behavior emerged as an important property of AC materials and defines the effect of rest period on rutting. The impact of rest period may diminish and become negligible at values above a certain threshold; however, the threshold is yet to be found. The extent of rest-period impact on AC depends on stress, temperature, AC characteristics, and rest period.

CHAPTER 3: IMPACT OF REST PERIOD ON PERMANENT DEFORMATION EXPERIMENTALLY

To accomplish the research objective, an experimental program was developed considering the effect of binder type and aggregate structure. The AC-mixture design variables, materials, and testing parameters, including rest period, temperature, and stress levels, were selected to identify the impact on AC permanent deformation.

EXPERIMENTAL PLAN

Materials and Mix Design

Two AC-mix designs were developed. Aggregate and asphalt binders were obtained from local suppliers in Arizona. First, a 1/2-in NMAS fine, dense-graded AC mix was acquired in accordance with Arizona Department of Transportation (ADOT) specifications. Aggregates were provided by the Vulcan Materials Company plant in the Phoenix area. These included the following stockpiles: 1/2-in coarse aggregate, 3/8-in coarse aggregate, crusher fines, washed crusher fine, and concrete sand. The two AC-mix designs include 1.0% lime in accordance with the region's moisture-sensitivity protocol. Four different types of binders were used in both AC mixes: PG 70-10, PG 76-22 TR+ (a combination of terminal blend rubber [TR] modification and Styrene-Butadiene-Styrene (SBS) to achieve the target grade), PG 76-22 SBS, and PG 64-28 SBS.

The key volumetric properties from the AC fine-mix design results were as follows: binder content 6.2% and voids in mineral aggregates (VMA) 16.3%. A 1/2-in NMAS coarse, dense-graded AC mix was developed using the same source materials in accordance with the Bailey method (Vavrik et al., 2001), where binder content 5.4% and VMA 14.6%. Both AC mixes were designed for 70 gyrations. The aggregate gradations are presented in Figure 14.

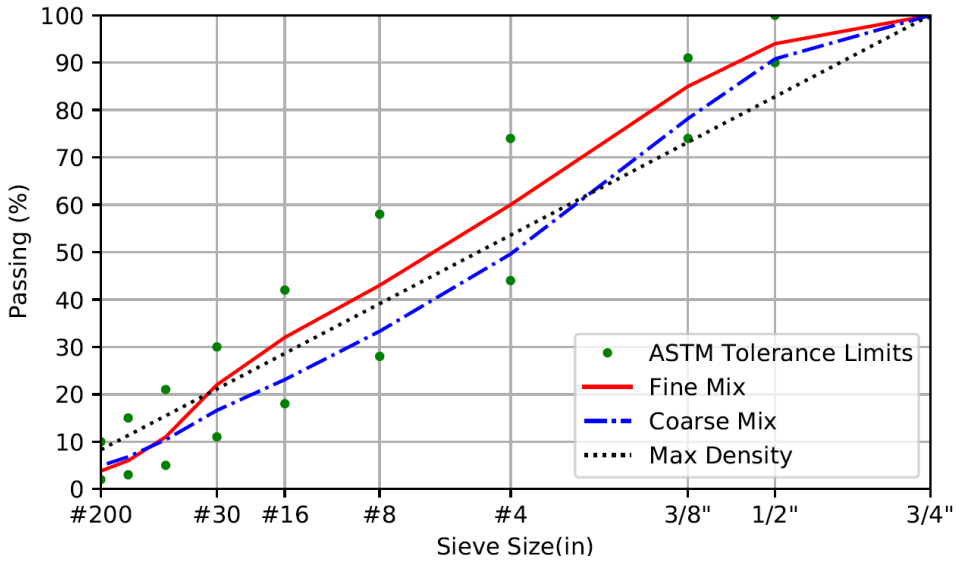

Figure 14. Graph. Aggregate gradation for coarse and fine dense-grade mix design.

Experimental Program

The experimental program is presented in Figure 15. Permanent-deformation characteristics were evaluated using the flow-number experimental setup in accordance with AASHTO T378, with modifications to incorporate rest periods as needed. The effect of three different stress levels and temperatures was coupled with the rest-period variable. In addition, the complex modulus and linear viscoelastic characteristics of each AC mixture with the four binders were determined. Standard and customized multiple-creep stress-recovery (MSCR) tests were performed on the binder to identify possible contribution of hardening–relaxation behavior of the binder on the AC permanent deformation. The details of each test are discussed in the following sections.

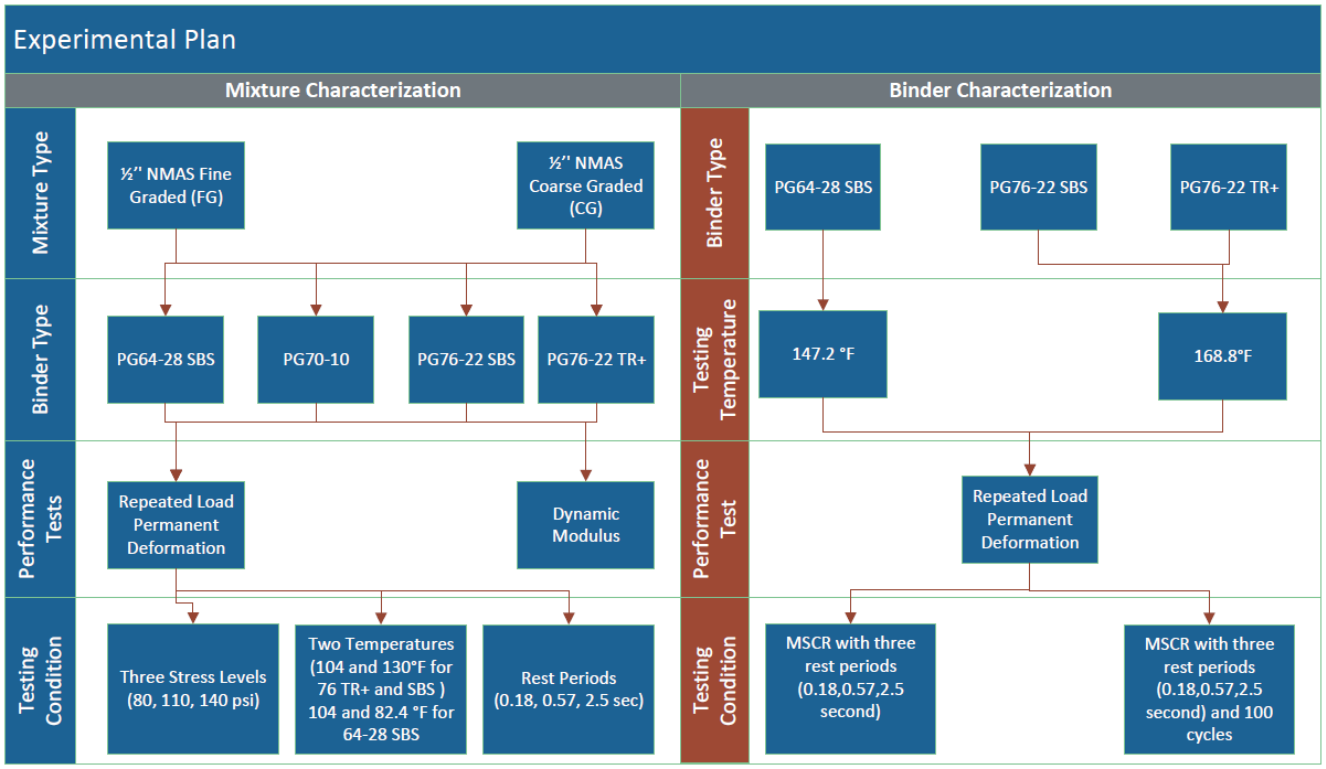

Figure 15. Illustration. Flowchart illustrating the experimental program.

Multiple-Stress Creep Recovery

MSCR tests were conducted in accordance with AASHTO T350 using two replicates of each binder type. In addition to the standard MSCR protocol, the samples were subjected to shear loads of 0.1 kPa (0.0145 psi) and 3.2 kPa (0. 465 psi) for 10 cycles with three rest periods (0.18, 0.57, and 2.5 sec). The samples were tested for 100 cycles at the same stress level. A combination of rest periods allowed investigation of the binders' response to cyclic loads beyond the binder linear viscoelastic range, which may contribute to hardening–relaxation.

Complex Modulus

Complex modulus tests were conducted in accordance with AASHTO T342. Three replicates were tested for each AC mixture. The target air void was 7 ± 0.5%. Controlled stress was used for all

specimens, generating a recoverable axial microstrain between 30 and 90 to ensure a linear relationship at different temperatures without damaging the specimens. The test was conducted at five temperatures (14°, 40°, 70°, 100°, and 130°F) and six frequencies (25, 10, 5, 1, 0.5, and 0.1 Hz). A 60-sec rest period was used between each frequency to allow for specimen recovery before applying the next loading at a lower frequency.

Repeated-Loading Permanent Deformation

Different pulse configurations were used to simulate the impact of potential truck-platoon scenarios on permanent deformation. The AASHTO T378 flow-number procedure was followed to prepare cylindrical AC specimens. The specimens were subjected to a haversine axial load without confinement. The cumulative permanent axial strains were recorded throughout the test. For each test configuration, two replicates from each AC mixture were produced and tested. The testing variables included loading time, temperature, and rest period, as presented in Table 2. The assumptions to select loading time and rest period are introduced in the following sections.

Selection of Loading Time

The loading time was determined based on the approach followed in AASHTOWare (Inc and ERES Division, 2004). The concept of pulse duration needed to calculate a representative viscoelastic modulus for AC layers was used. The steps to calculate pulse duration included factors such as traffic speed, depth of AC layer, tire radius, and single-tire wheel load (Inc and ERES Division, 2004). The assumptions made for these factors were as follows: a speed of 60 mph to simulate average highway speed in the United States, a single-tire wheel load of 9,000 lb, and a tire radius of 6 in. The AC layers were assumed to be 14-in thick, with three AC layers (wearing, intermediate, and base-AC), considering an interstate high-volume road scenario. Based on the effective depth assumption made in AASHTOWare, a pulse duration on the surface and in the AC base layer could be as low as 0.04 sec and 0.10 sec, respectively. Pulse durations of 0.05 sec and 0.10 sec were selected in the study. The experimental program included a rutting scenario for critical surface layers, conducted for a pulse duration of 0.05 sec. The impact of loading and its interaction with rest period are part of ongoing research.

Selection of Rest Period

The rest periods selected in this study were based on the safe sight distance between the trucks and an assumed highway truck-traffic speed of 60 mph. Three scenarios of distances between trucks were considered to simulate actual traffic conditions. A distance of 220 ft was chosen to simulate a typical safe sight distance between trucks, whereas 50 and 16 ft were chosen to simulate platoon distances. These distances corresponded to 2.5, 0.57, and 0.18 sec of rest periods, respectively. Additional extended rest periods up to 5 and 10 sec were tested with limited specimens to verify the extent of the impact of the rest period.

Selection of Temperature

Three temperatures were selected to simulate the critical environmental conditions in various climatic regions in the United States, such as Phoenix and Chicago. The temperatures selected were 130°F, 104°F, and 82.4°F. Each AC mixture was tested against at least two temperatures, based on the

high-temperature grade of the binder. An overlap of a minimum of one temperature was considered between AC mixes having different binder grades.

AC Air Voids

The primary stage of the densification process occurred during the first few months after the AC placement and opening for traffic. To simulate the most critical conditions in the primary and secondary stages of rutting, specimens were compacted at an air void of 7 ± 0.5%. In addition, a limited number of tests was conducted at an air void of 4 ± 0.5% to investigate the role of aggregate structure on rest period.

Table 2. Repeated-Load Permanent-Deformation Testing Matrix

Binder Type	Temperature (°F)	Mix Type	Test Matrix			
			Stress Level (psi)	Rest Period (sec)		
				0.18	0.57	2.5
PG 76-22 TR+	130	Fine	140			
PG 76-22 TR+	130	Fine	110			
PG 76-22 TR+	130	Fine	80			
PG 76-22 TR+	130	Coarse	140			
PG 76-22 TR+	130	Coarse	110			
PG 76-22 TR+	130	Coarse	80			
PG 76-22 TR+	104	Fine	140			
PG 76-22 TR+	104	Fine	110			
PG 76-22 TR+	104	Fine	80			
PG 76-22 TR+	104	Coarse	140			
PG 76-22 TR+	104	Coarse	110			
PG 76-22 TR+	104	Coarse	80			
PG 76-22 SBS	130	Fine	140			
PG 76-22 SBS	130	Fine	110			
PG 76-22 SBS	130	Fine	80			
PG 76-22 SBS	130	Coarse	140			
PG 76-22 SBS	130	Coarse	110			
PG 76-22 SBS	130	Coarse	80			
PG 76-22 SBS	104	Fine	140			
PG 76-22 SBS	104	Fine	110			
PG 76-22 SBS	104	Fine	80			
PG 76-22 SBS	104	Coarse	140			
PG 76-22 SBS	104	Coarse	110			
PG 76-22 SBS	104	Coarse	80			
PG 70-10	130	Fine	140			
PG 70-10	130	Fine	110			
PG 70-10	130	Fine	80			
PG 70-10	104	Fine	140			
PG 70-10	104	Fine	110			
PG 70-10	104	Fine	80			
PG 64-28 SBS	104	Fine	140			
PG 64-28 SBS	104	Fine	110			
PG 64-28 SBS	104	Fine	80			
PG 64-28 SBS	104	Coarse	140			
PG 64-28 SBS	104	Coarse	110			
PG 64-28 SBS	104	Coarse	80			

Binder Type	Temperature (°F)	Mix Type	Test Matrix			
			Stress Level (psi)	Rest Period (sec)		
				0.18	0.57	2.5
PG 64-28 SBS	82.4	Fine	140			
PG 64-28 SBS	82.4	Fine	110			
PG 64-28 SBS	82.4	Fine	80			
PG 64-28 SBS	82.4	Coarse	140			
PG 64-28 SBS	82.4	Coarse	110			
PG 64-28 SBS	82.4	Coarse	80			

RESULTS AND DISCUSSION

Multiple-Stress-Creep Recovery

The results from the standard MSCR experiments from the first 10 cycles are presented in Table 3. It is demonstrated that SBS-modified binders (PG 76-22 and PG 64-28) performed similarly in terms of their recovery characteristics and irrecoverable creep compliance (Jnr). The binder PG 76-22 TR+ had a lower recovery percentage and higher Jnr than the other binders, perhaps suggesting a higher permanent-deformation susceptibility under repeated loads. Increasing the rest period had a significant and consistent effect on both recovery percentage and Jnr for the three binders. Increasing rest period resulted in improved recovery percentage and a reduction in Jnr, indicating a greater permanent-deformation resistance. As the rest period increased, recovery of viscoelastic strains continued, resulting in less accumulated permanent deformation.

Table 3. Recovery and J_{nr} Properties of Various Binders at Variable Rest Periods (1 kPa = 0.145 psi)

Binder Type	Temperature (°F)	Parameter (%)	Rest Periods (sec)		
			0.18	**0.57**	**2.5**
PG 76-22 SBS	168.8	Recovery at 0.1 kPa	42.2	63.7	81.7
PG 76-22 SBS	168.8	Recovery at 3.2 kPa	10.2	20.1	33.6
PG 76-22 SBS	168.8	Jnr at 0.1 kPa	1	0.7	0.5
PG 76-22 SBS	168.8	Jnr at 3.2 kPa	3.2	2.6	2.1
PG 76-22 TR+	168.8	Recovery at 0.1 kPa	16.1	28.5	42.6
PG 76-22 TR+	168.8	Recovery at 3.2 kPa	1.9	4	6.8
PG 76-22 TR+	168.8	Jnr at 0.1 kPa	3	2.8	2.5
PG 76-22 TR+	168.8	Jnr at 3.2 kPa	5.7	5.7	5.5
PG 64-28 SBS	147.2	Recovery at 0.1 kPa	44.7	70.1	93
PG 64-28 SBS	147.2	Recovery at 3.2 kPa	18.4	37.6	60.7
PG 64-28 SBS	147.2	Jnr 0.1 at kPa	0.6	0.4	0.1
PG 64-28 SBS	147.2	Jnr 3.2 at kPa	1.3	0.9	0.6

The next step was to test if the same trend would continue for an extended number of cycles; the binder in the AC mixture would be subjected to more cycles in a permanent-deformation experiment. Figure 16 presents the results at varying rest periods for 100 cycles. As the rest period increased, accumulated shear strain decreased for PG 76-22 SBS, as presented in Figure 16. a. Once again, that

effect could be attributed to the increasing percentage of recoverable strains after each cycle with a longer rest period. Figure 16. b presents a comparison of the three binders at 2.5 sec of rest period. The SBS modified binders ranked consistently better than the terminal-blend rubber and SBS combination (PG 76-22 TR+) at all stress levels and rest periods.

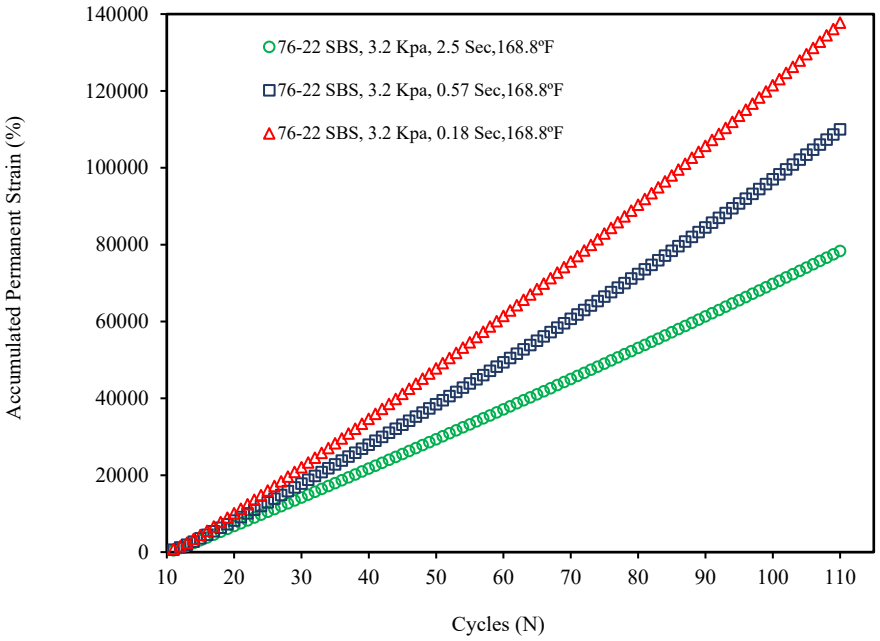

A. Three rest periods (0.18, 0.57, and 2.5 sec) for PG 76-22 SBS

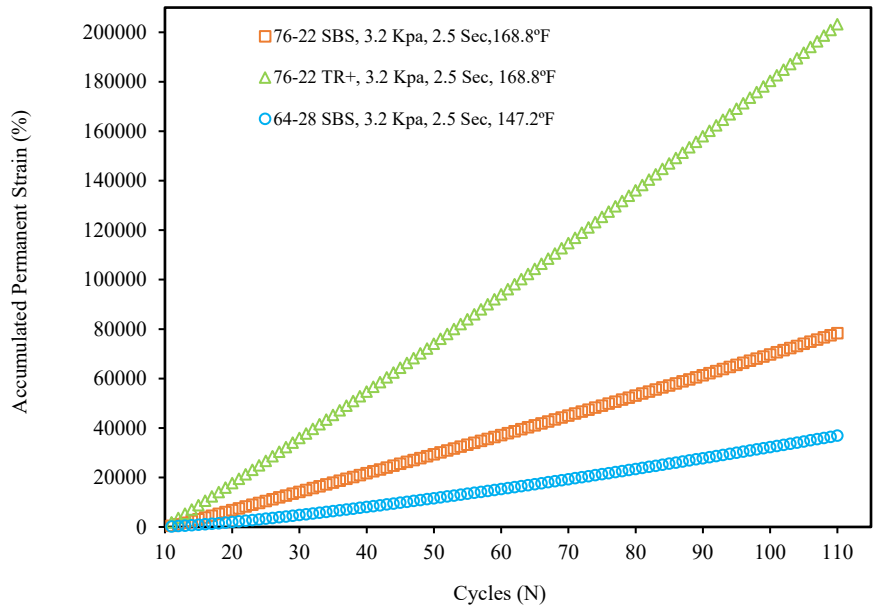

B. Rest period (2.5 sec) for PG 76-22 SBS, PG 76-22 TR+, and PG 64-28 SBS

Figure 16. Graphs. Accumulated permanent deformation based on 100 cycles, 3.2 kPa (1kPa= 0.145 psi) in MSCR test.

Complex Modulus Results

The complex modulus master-curve plots were constructed by shifting results to the reference temperature of 70°F. The complex modulus and phase-angle results were analyzed to present master curves and black-space graphs, as presented in Figure 17. and Figure 18. , respectively. The results obtained included the fine- and coarse-graded AC mixes prepared with the three types of binders (PG 76-22 SBS, PG 76-22 TR+, and PG 64-28 SBS). The fine-graded AC mixes with PG 76-22 SBS and PG 76-22 TR+ had similar modulus values, whereas the AC mix with PG 64-28 SBS had a lower modulus at reduced frequencies (i.e., lower than 10 Hz). The same trend could be observed for the coarse-graded AC mixes. However, the coarse-graded mix for all three binders showed a relatively higher complex modulus at higher reduced frequencies. The difference could be attributed to the aggregate gradation and lower VMA of the coarse-graded AC mix.

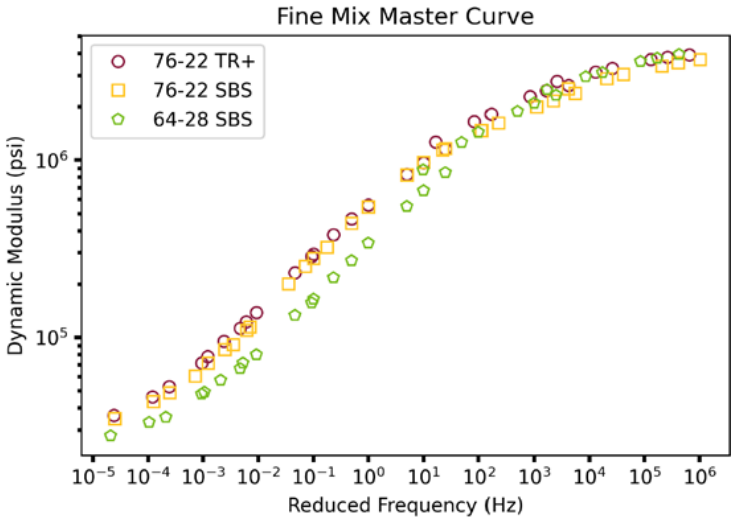

A. Fine-graded AC mix

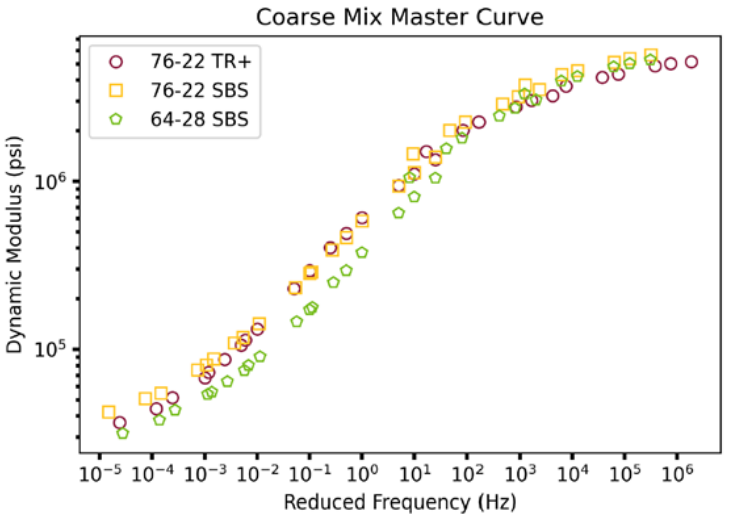

B. Coarse-graded AC mix

Figure 17. Graphs. Master curves for both fine-graded AC mix and coarse-graded AC mix.

The black-space plots show the relationship between the complex modulus and phase angle. No significant difference in the black space could be observed when binder type was altered for both coarse- and fine-graded AC mixes.

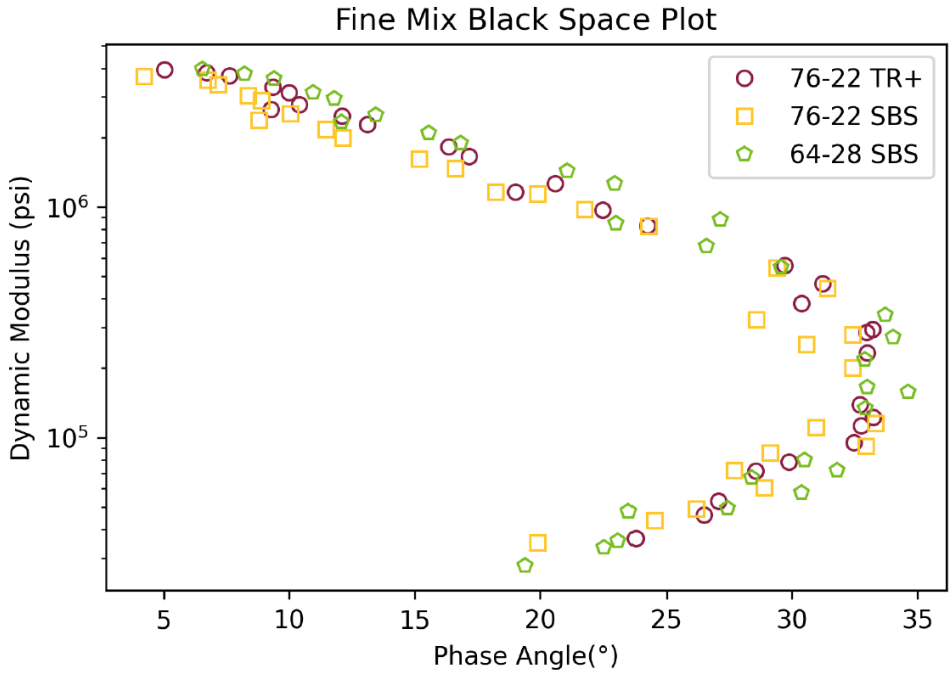

A. Black space of fine-graded mix

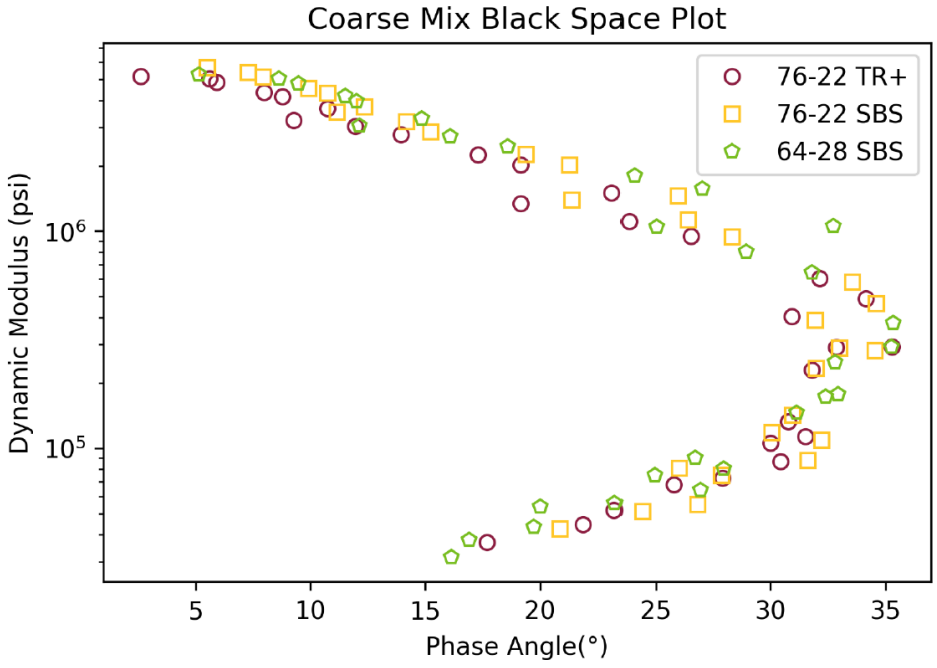

B. Black space of coarse-graded mix

Figure 18. Graphs. Black space for both fine-graded mix and black space of coarse-graded mix.

Repeated-Loading Permanent-Deformation Results

The results of the flow-number test conducted at 104°F for the fine-graded AC mix using the four binder types are presented in Figure 19. The AC permanent deformation increased with when the rest period increased, independent of the binder type. The impact of the rest period at the AC-mixture level was contrary to that measured on the binder; however, AC mixture test was consistent with results reported elsewhere in the literature (Darabi et al., 2013; Yun and Kim, 2011; Motevalizadeh et al., 2018). As would be expected, the AC mix with PG 76-22 SBS showed the best performance to resist permanent deformation.

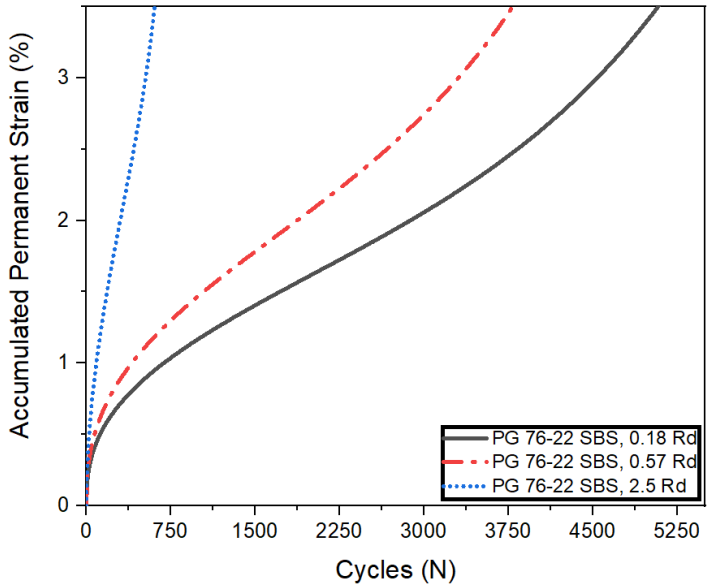

A. Effect of rest period based on 140 psi, 104°F for PG 64-28 SBS

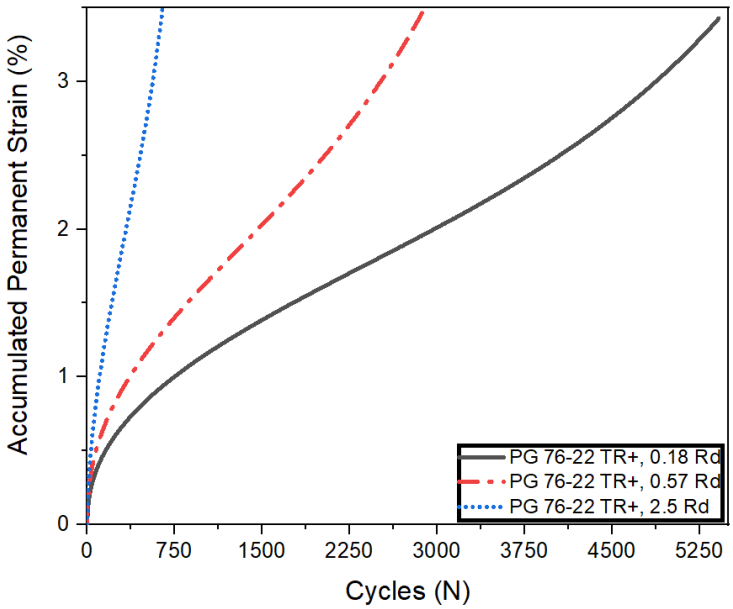

B. Effect of rest period based on 140 psi, 104°F for PG 76-22 TR+

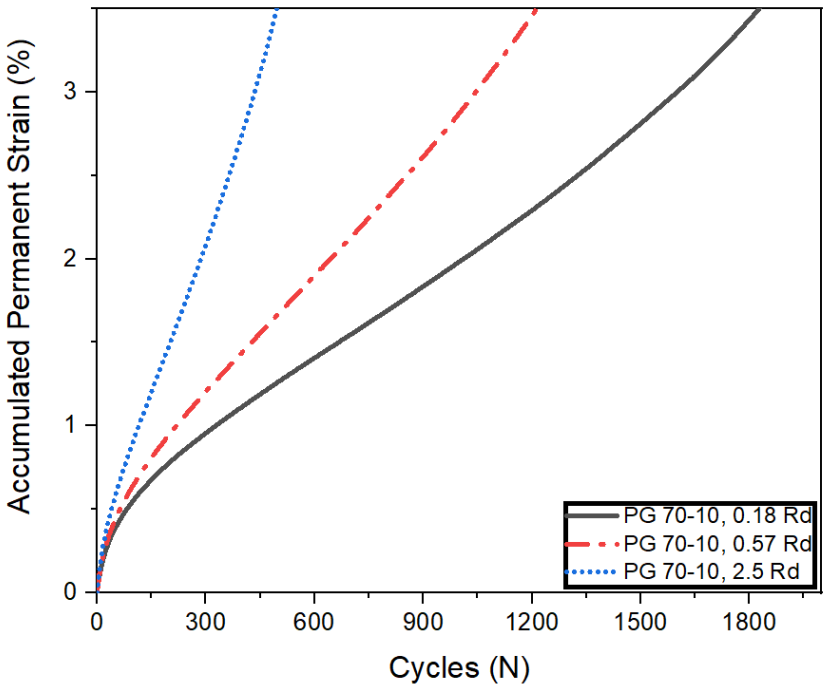

C. Effect of rest period based on 140 psi, 104°F for PG 70-10

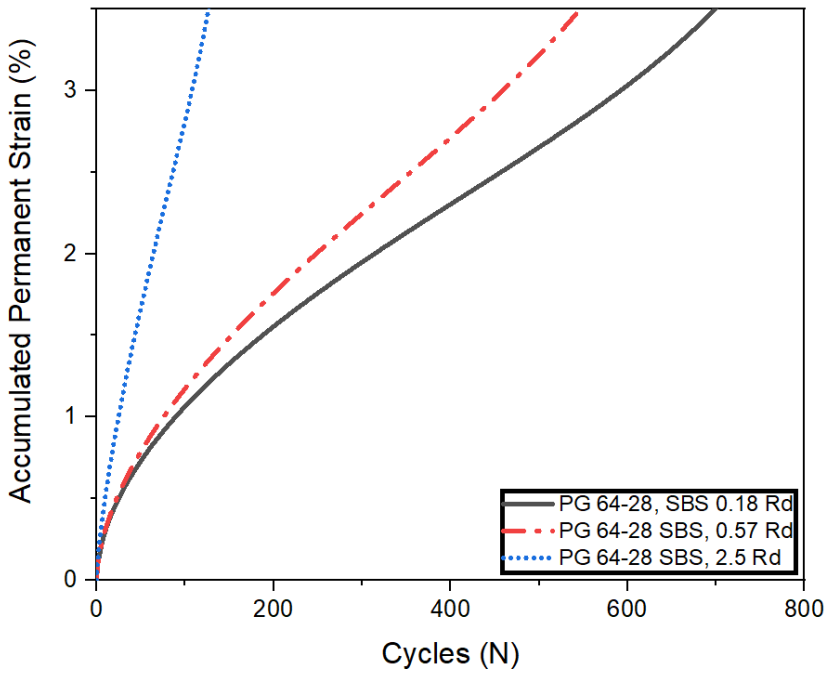

D. Effect of rest period based on 140 psi, 104°F for PG 64-28 SBS

Figure 19. Graphs. Effect of rest period based on 140 psi, 104°F and four binder types for fine-graded AC mixes.

Figure 20. shows the permanent-deformation results for the coarse-graded AC mix utilizing two binder types at 130°F. The same trend of increasing permanent deformation with increasing rest period was observed. Additional tests were conducted at extended rest periods for the AC mix with PG 76-22 TR+ (Figure 20. a). Permanent deformation continued to increase with rest period up to 10 sec. However, it can be observed that the rest period impact slowly diminished after 2.5 sec.

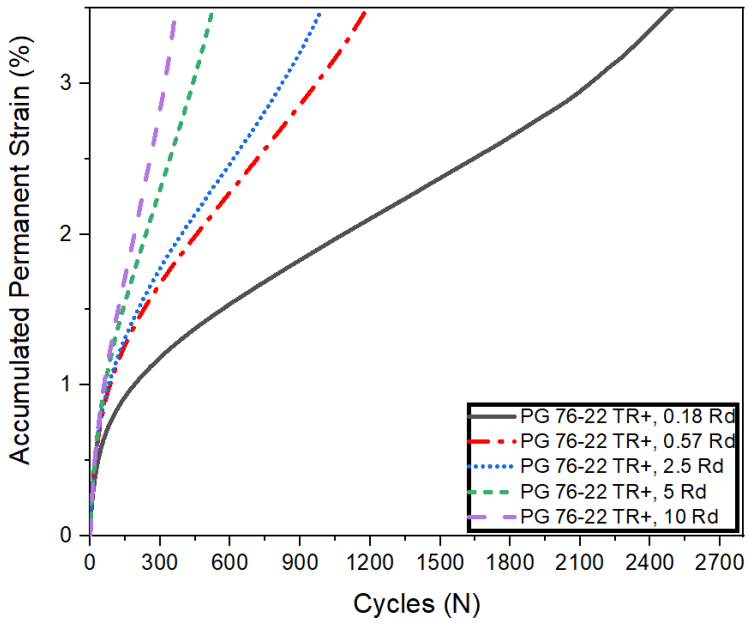

A. Effect of rest period based on 110 psi, 130°F PG 76-22 TR+

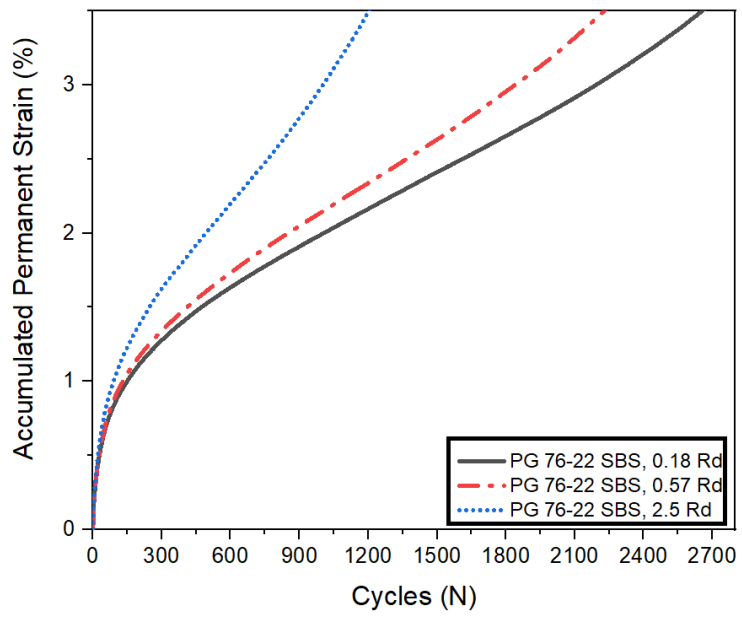

B. Effect of rest period based on 110 psi, 130°F and PG 76-22 SBS

Figure 20. Graphs. Effect of rest period based on 110 psi, 130°F for coarse-graded AC mixes.

Flow numbers were calculated for each test and are presented in Figure 21. a for the fine-graded AC mix at 104°F and 110 psi. The mix with PG 76-22 SBS had the highest flow number, while PG 64-28 had the lowest flow number. The impact of rest period was clearly observed with the flow numbers. Normalized flow numbers are presented in Figure 21. b, using the same data to investigate the behavior of various binder grades. Despite a few small differences in the slope of the normalized curves, the behavior was consistently defined by an exponential decline. The reduction in the flow number was in the range of 20% to 30% when the rest period was increased to 0.57 sec from 0.18 sec. When the rest period increased up to 2.5 sec, the flow number decreased by about 70% to 80%. Considering the variability in data, it could be argued that binder-grade effect relative to rest period on AC permanent deformation was low. It is worth noting that by changing rest period in the experiment, the effect of binder on AC performance could be controlled, achieving comparable performance of SBS-modified and unmodified binders. This observation is important in selecting the combination of testing parameters that include not only temperature and stress level but also rest duration.

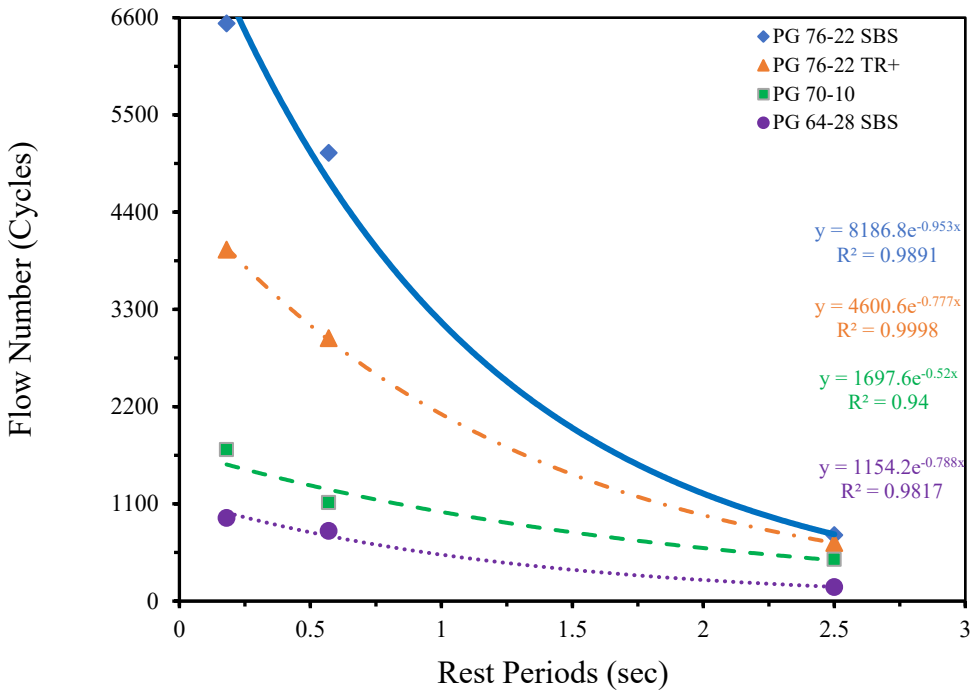

A. Effect of rest period based on flow number at 104°F

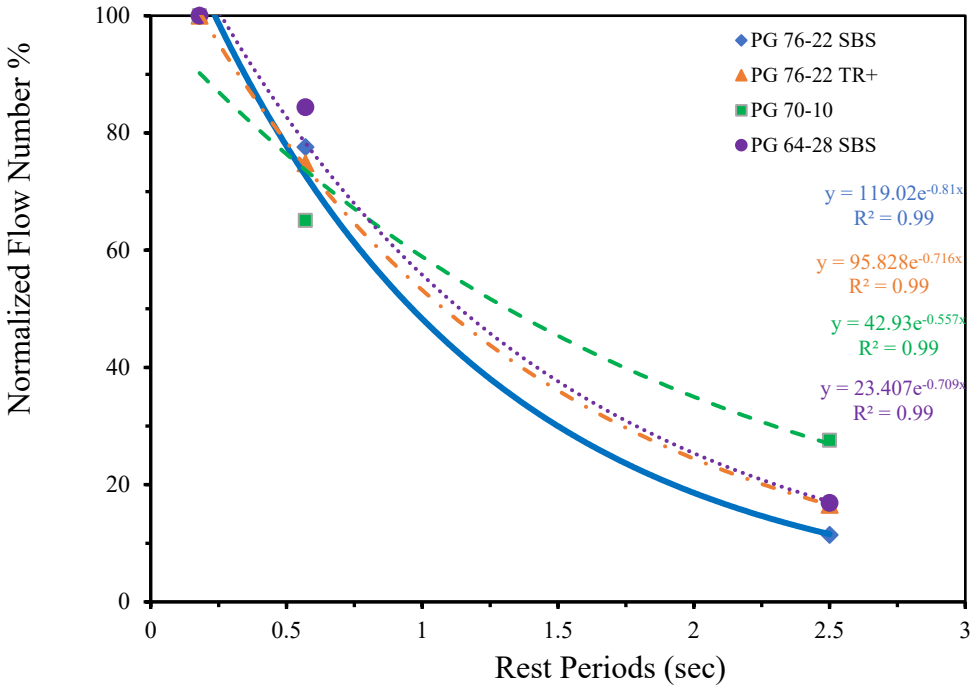

B. Effect of rest period based on normalized flow number at 104°F

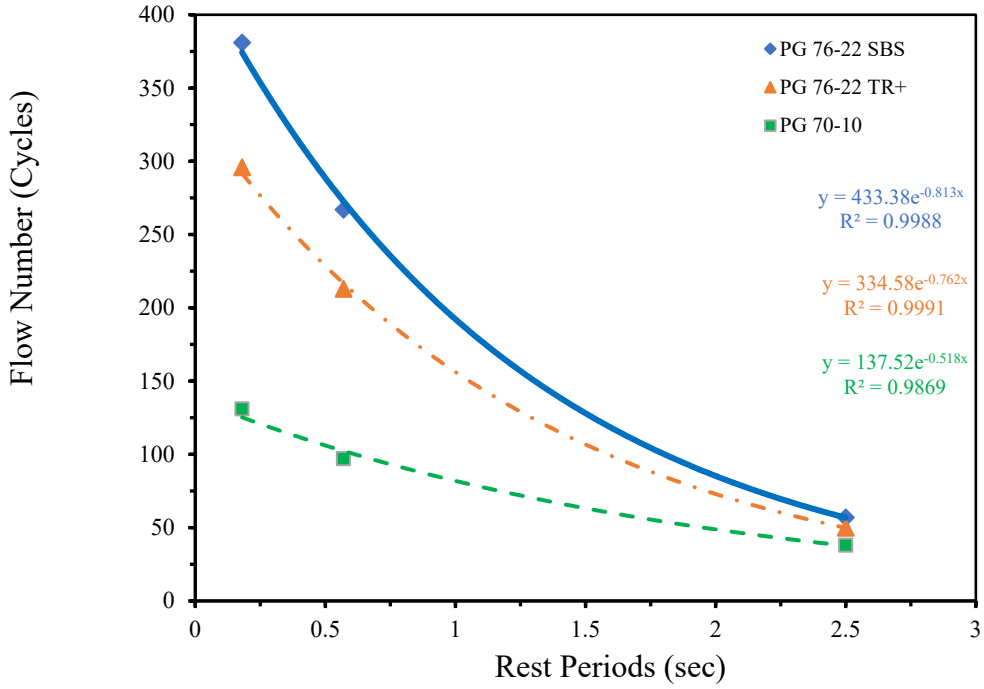

C. Effect of rest period based on flow number at 130°F

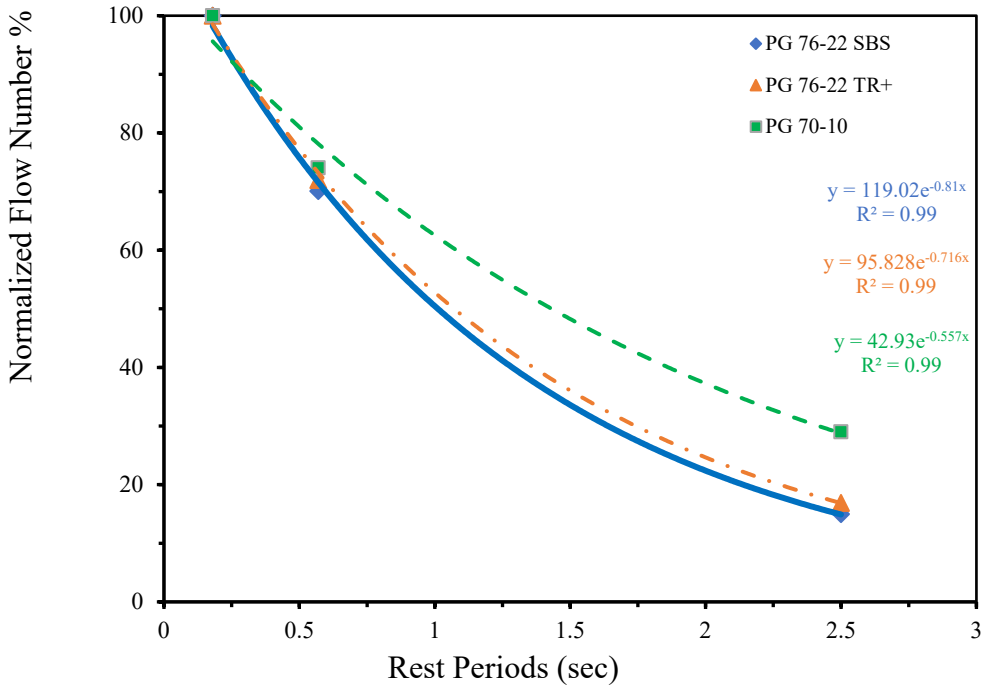

D. Effect of rest period based on normalized flow number at 130°F

Figure 21. Graphs. Effect of rest period based on 110 psi for four different types of binders.

A similar analysis was conducted to evaluate the effect of stress level. Figure 22 presents the flow number and normalized flow number for the four binder grades. Stress level was added to the testing matrix to mimic the effect of traffic wander. A similar exponential decline could be observed with the flow number and stress-level relationship. At each stress level, the AC mixes with PG 76-22 SBS and PG 76-22 TR+ outperformed the rest of the AC mixes; the AC mix with PG 76-22 SBS showed the best performance. A relative reduction in the flow number (Figure 22b) showed consistent exponential decline similar to that of the rest-period impact presented in Figure 21. b. A greater reduction was observed in the stress change from 80 psi to 110 psi than the stress-level increase from 110 psi to 140 psi. That difference could be explained by increasing nonlinearity with increasing stress level. However, a greater percentage of reduction was observed with the two top-performing binders (about 70% to 90% for the two stress levels, respectively) than with the other two (about 40% to 80% for the two stress levels, respectively). The AC mixes might be reaching a limit state of yielding governed by factors other than the stress level.

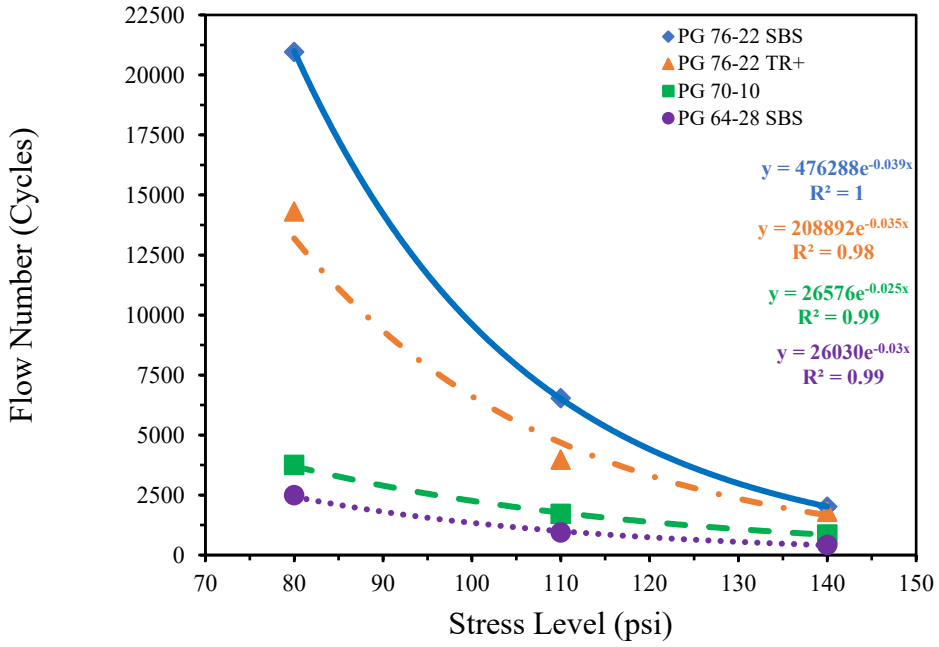

A. Effect of stress level based on flow number

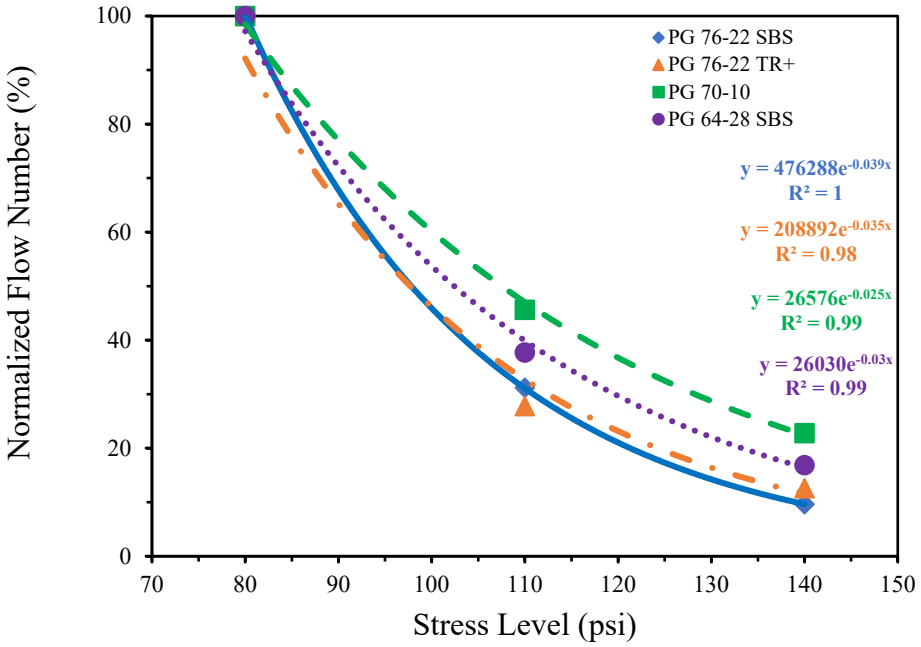

B. Effect of stress level based on normalized flow number

Figure 22. Graphs. Effect of stress level based on 0.18-sec rest period and 104°F for four binders.

Lastly, the impact of the rest period based on aggregate gradation and density was evaluated. Figure 23 presents the number of cycles to reach a 3% permanent strain for the fine- and coarse-graded AC mixes at 7% air void. The coarse-graded AC mixture was also prepared at a reduced air void (4%) to check if changing the aggregate skeleton may alter the trends with the observed rest period. The coarse-graded AC mix showed higher resistance to permanent deformation than the fine-graded AC mix at all rest periods. The impact of the rest period was shown to be consistent for both AC mixes. As would be expected, the coarse-graded AC mix at a reduced air void had the highest resistance to permanent deformation. However, permanent-deformation resistance was significantly reduced with increasing rest period, as observed experimentally.

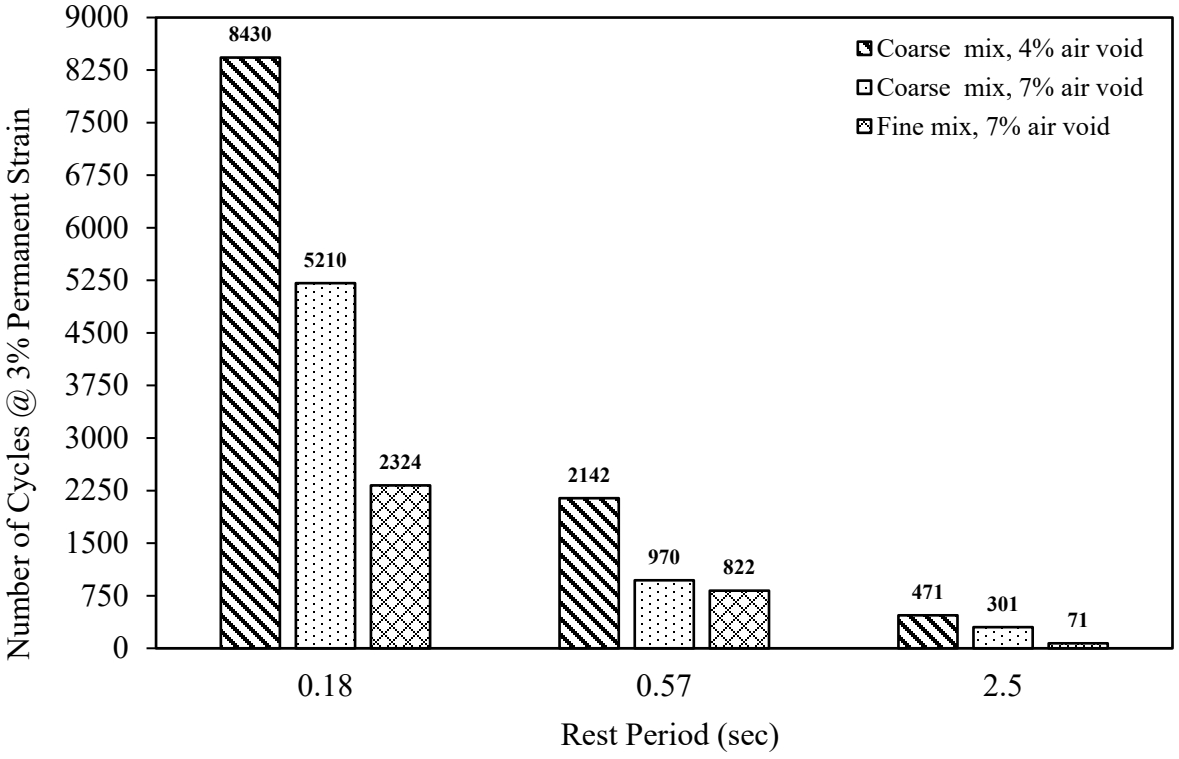

Figure 23. Graph. Effect of aggregate skeleton and air void based on 130°F and 110 psi for PG 76-22 TR+.

SUMMARY

An experimental program was performed to understand the impact of rest period on AC permanent deformation. The experimental variables included stress level, temperature, and rest period. Two types of AC mixes, fine- and coarse-graded, were tested using four binder grades. The study concluded that although increasing rest period would increase binder permanent-deformation resistance when tested in the shear mode, the opposite trend was observed for AC mixes mainly due to the aggregate structure and compression loading. The linear viscoelastic recovery characteristics

governed deformation behavior of the binder, which resulted in reduced total deformation with increasing rest period.

For AC mixes, increasing rest periods from 0.18 to 2.5 sec increased permanent deformation consistently under testing conditions applied in this study. The reduction in the flow number with an increase in rest period from 0.18 to 2.5 sec could be as high as 80%. The hardening–relaxation, or hardening–softening, mechanism proposed in the literature was consistent with the experiments conducted in this study when specimens were loaded axially. The impact of rest period was consistent for coarse- and fine-graded mixes and the mix at the reduced air-void content. The reduction in permanent-deformation resistance with increasing rest period was shown to be comparable to a change in stress level by about 65.3 psi. Rest-period influence on permanent deformation diminishes beyond 2.5 sec.

CHAPTER 4: MECHANISTIC MODEL DEVELOPMENT

In a study conducted by Choi and Kim (2013), a *shift model* was proposed to include the effects of deviatoric stress, temperature, and loading time on permanent deformation. The shift model is based on superposition principles of time–temperature and time–stress. The main objective of the study was to develop a single master curve for permanent deformation that comprises the effect of stress level, loading time, and temperature. The benefit of this approach is that the permanent deformation can be computed for any new stress level, loading time, and/or temperature using shift factors that are computed from shift functions. The coefficients of shift functions are obtained by shifting the actual experimental data. The procedure is similar to developing a master curve from dynamic modulus experiments. Similarly, for this study, permanent-deformation curves were shifted with respect to a reference rest period. A master curve for permanent deformation as a function of rest period was developed.

SHIFTING CURVES FOR REST PERIOD

The experimental data were used to develop a master curve for permanent deformation as a function of rest period. The curves could not be shifted directly; shape changed with load-cycle applications. Each curve has three parts, commonly known as primary (R1), secondary (R2), and tertiary (R3) regions (Figure 24.). The primary region represents the densification of the AC layer due to initial traffic-load application. Permanent deformation would be similar for all rest periods in the primary region. As specimens were loaded until failure, tertiary regions were observed. A pavement section is considered to have failed if permanent strain reaches the tertiary region. The tertiary region is where material is considered to be in the flow state. Therefore, pavement-design guidelines often overlook primary and tertiary regions for the rutting analysis. In PMED, the permanent-strain function is used to capture mainly the behavior of the secondary region, where accumulation of rutting occurs. Hence, before shifting the experimental data directly, preprocessing of the experimental data was needed.

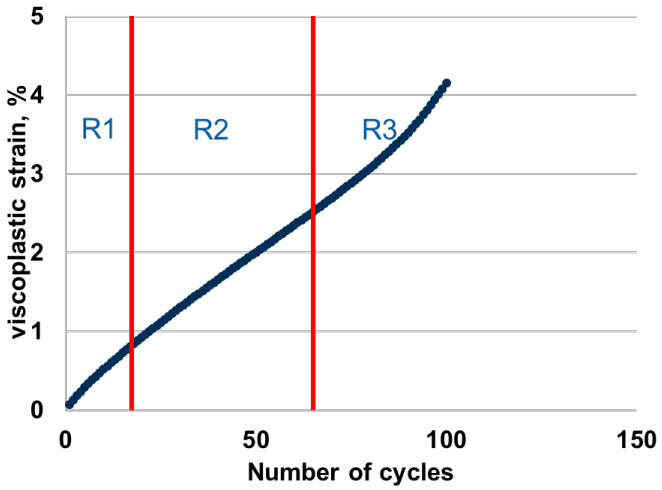

Figure 24. Illustration. Primary, secondary, and tertiary regions in a strain curve.

The curvature changes from convex to concave while transitioning from secondary to tertiary regions. The point where the tertiary region starts in the curve is known as the flow-number (FN) point. In the secondary region, strain increases at a slower rate (a power function), as compared to an exponential rate in the tertiary region. The experimental data was fitted with a Franken model, as presented in Figure 25. .

$$\epsilon_p = AN^B + C(e^{DN} - 1)$$

Figure 25. Equation. Franken model.

where ϵ_p= permanent deformation or plastic strain; N = number of loading cycles; and A, B, C, and D = regression constants obtained from fitting the equation with experimental data. The FN point is determined by computing the number of cycles for which the double derivative of the equation (Figure 25.) is zero. Hence, the region past the FN point is removed during the analysis. As there is no clear transition point from primary to secondary region, a strain threshold was set to eliminate the primary region. Strain threshold was selected based on the extent of overlapping for all the curves during the initial cycles of loading. The procedure is presented systematically in Figure 26. for binder PG 64-28 SBS at 104°F with loading of 80 psi. In Figure 26. A, three red circles on strain curves represent the FN point computed from the Franken model. Tertiary data was removed, and 0.75% ϵ_p was set to exclude the primary region (Figure 26. B). The FN points are different for different rest periods (Figure 26. A). Hence, the extent of data that could be used for shifting was determined by the curve with the lowest FN (occurs at highest rest period). Therefore, another vertical red dashed line is presented in Figure 26. B. The region between the two vertical dashed lines (number of cycles) is the data that could be used for shifting. The final preprocessed data are presented in Figure 26. C.

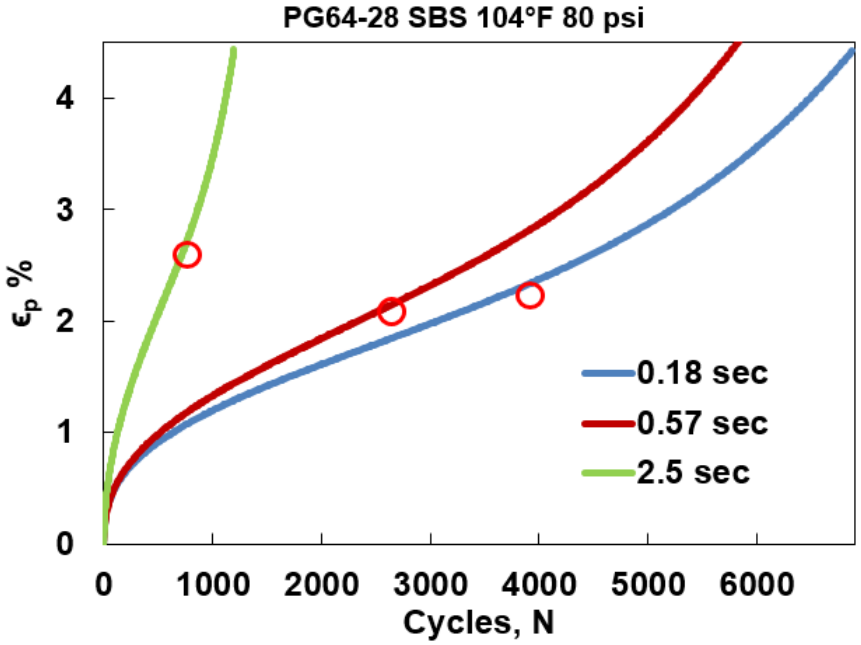

A. Strain curves with FN points

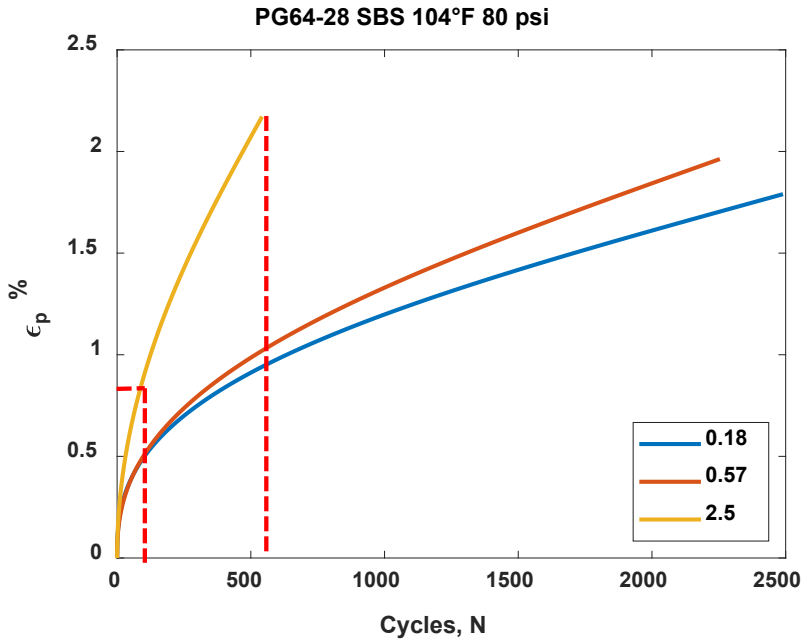

B. Removal of tertiary and setting threshold for primary region

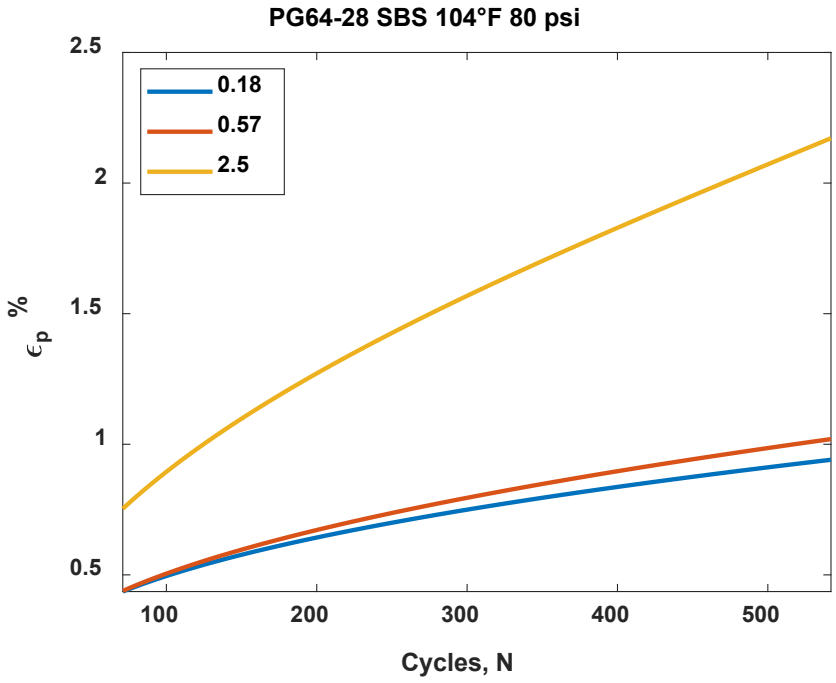

C. Final preprocessed data

Figure 26. Plots. Schematic representation of preprocessing experimental data for shifting.

After preprocessing (Figure 26. C), data were shifted in the log space similar to complex modulus to the reference curve. The strain curve for the 0.18-sec rest period was taken as a reference. The final shifted curve is shown in the Figure 27. For example, if it takes 1,800 cycles to reach 1.75% strain for a rest period of 0.18 sec, it will take only 400 cycles to reach the same strain for 2.5 sec. The Williams-

Landel-Ferry (WLF) equation was used to compute the shift factors. In general, the WLF equation was used to compute shift factors for complex modulus data. Temperature was replaced with rest period (RP) in the equation (**Figure 28.**).

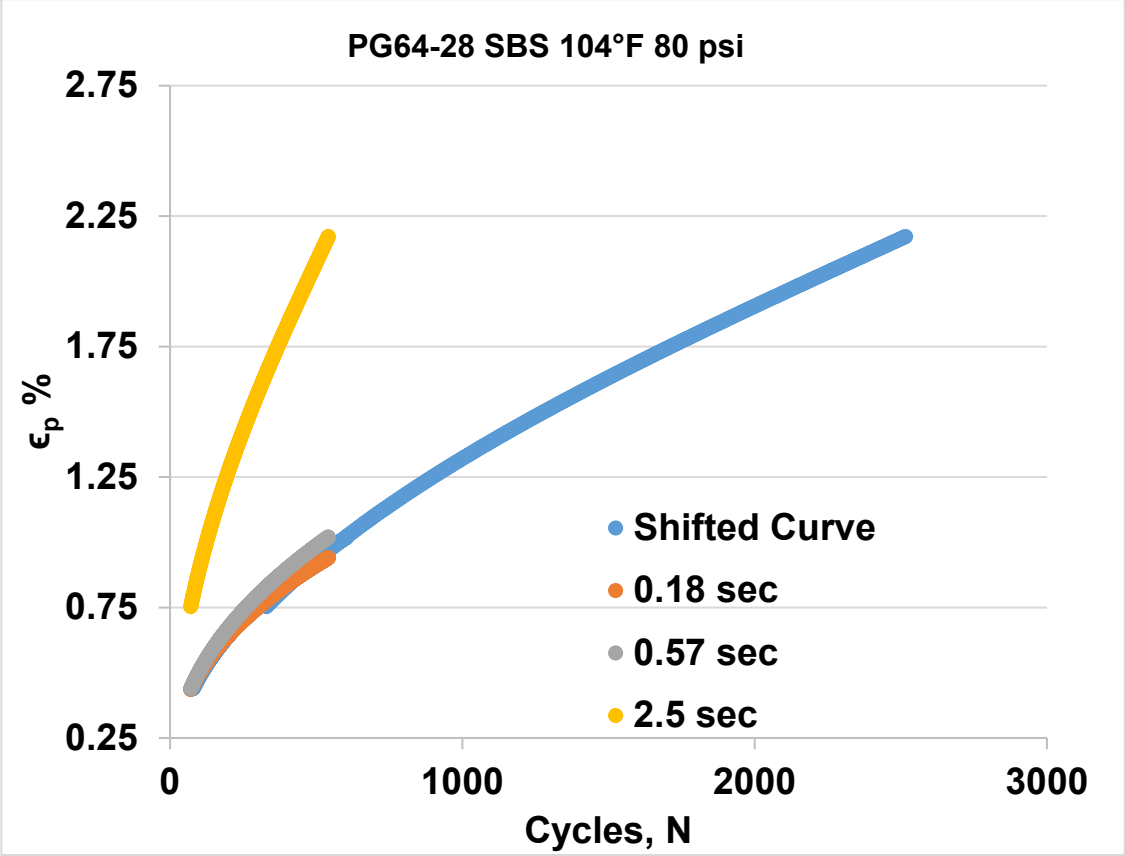

Figure 27. Plot. Shifted curve of experimental data.

$$log(\mathrm{a_T}) = \frac{-\mathrm{C_1}(RP - \mathrm{RP_{ref}})}{\mathrm{C_2} + (\mathrm{RP\text{-}RP_{ref}})}$$

Figure 28. Equation. Shift function for rest-period data.

where, a_T is shift factor; C_1, C_2 are coefficients of shift function; RP is rest period; and RP_{ref} is reference rest period. Coefficients of shift functions were computed using the experimental data. Once coefficients were determined, shift factors could be computed for any rest period. Hence the strain curve could be obtained for newer rest periods without conducting further experiments. To verify the rest-period effect on strain and data shifting, additional tests were conducted with rest periods of 1 and 1.5 sec for PG 76-22 SBS 130˚F at 110 psi loading. The data were initially preprocessed and shifted with only four rest periods (0.18, 0.57, 2.5, and 1.5 sec), with the curve for the 1.5-sec rest period as reference. Coefficients C_1, C_2 were calculated using actual data, and the shift factor for the 1-sec rest period was computed. The strain curve was generated using the computed shift factor and was compared with actual experimental data (Figure 29.). Predicted and

experimental values matched closely, and this approach appeared to be an appropriate technique to quantify the rest-period effect.

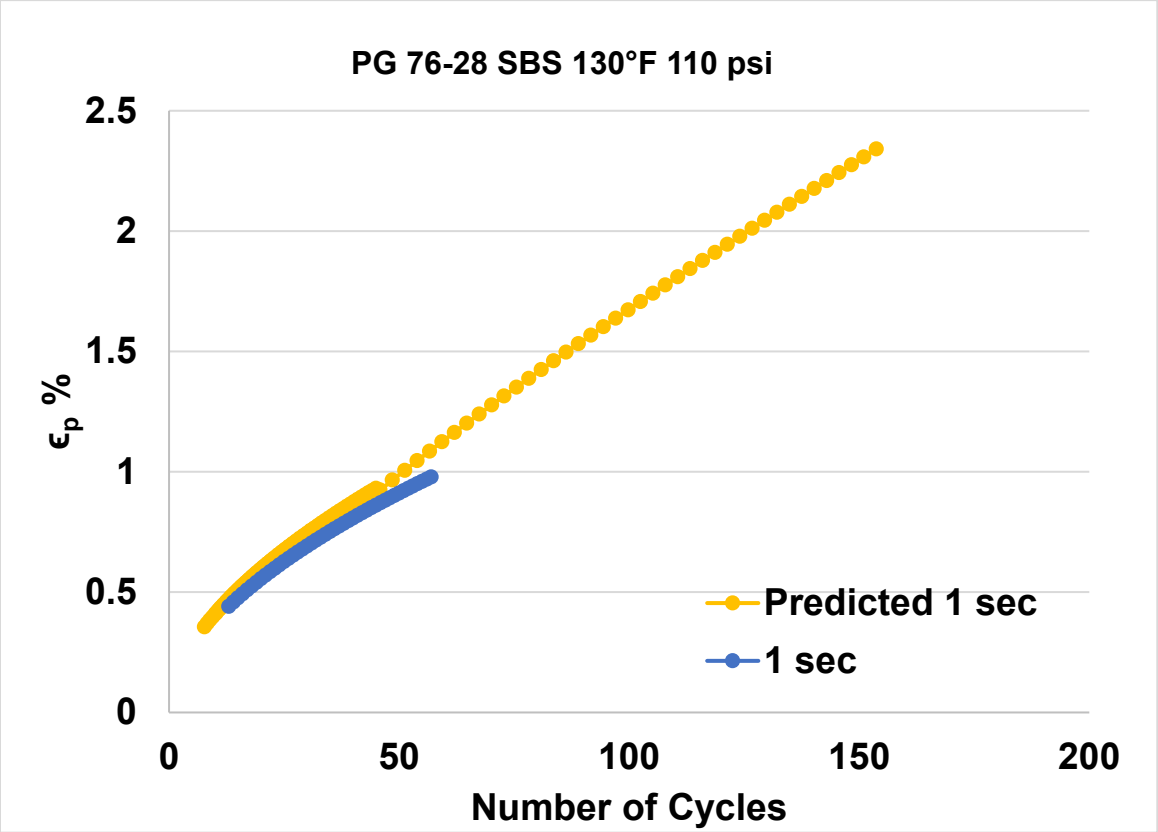

Figure 29. Plot. Predicted and experimental data for 1-sec rest period.

CORRECTION-FACTOR DEVELOPMENT

Currently, the PMED program does not consider the influence of rest period. In PMED, pavement is divided into sublayers; and vertical compressive strains are obtained at mid-depth of each sublayer using linear elastic analysis. Rutting is calculated for all sublayers using the transfer function. Transfer functions are different for bound and unbound materials. Total rutting in the pavement is simply the summation of all rut in the sublayers. The effect of rest period on unbound materials is beyond the scope of this study. Therefore, correction factors were provided only for AC layers. The transfer function used in PMED for a given sublayer is presented in Figure 30. .

$$\delta_{\text{sub}} = f(sublayer) \times N^{\text{b}}$$

Figure 30. Equation. Rutting equation for an AC sublayer

where, δ_{sub} is rut on the specific sublayer; $f(sublayer)$ is function of sublayer thickness, depth of sublayer from pavement surface, compressive strain, global and local calibration factors, and temperature at sublayer; N is number of load repetitions; and b is a calibration constant. It is to be

noted that for each sublayer $f(sublayer)$ needs to be computed separately. The effect of rest period can be incorporated simply by changing the number of load repetitions. The correction factor would be a_T obtained from **Figure 28.** for a newer rest period. The equivalent number of repetitions would be calculated as presented in Figure 31. .

$$N_{eq} = \frac{N}{a_T}$$

Figure 31. Equation. Equivalent number of load repetitions.

where, N_{eq} is the equivalent number of load repetitions, N is number of repetitions for the reference rest period, and a_T is the computed shift factor. Temperature and load-level change along the depth of the pavement; and hence, values will be different for each sublayer. It is a well-established fact, and observed in this study, that stress level and temperature have significant impact on the permanent deformation during experiments. Therefore, N_{eq} is different for each sublayer. Hence, a_T should be a function of rest period, as well as load level and temperature. The experiments were conducted for three stress levels and two temperatures. Hence, shift factor could be computed approximately as a function of stress level and temperature. The coefficients of shift function for all tests conducted for AC mix with PG 64-28 SBS are presented in Table 4.

Table 4. Coefficients of Shift Function (See Figure 28.)

Temperature	**104°F**		**82°F**	
Stress Level (psi)	**C_1**	**C_2**	**C_1**	**C_2**
80	-457.93	1617.58	-524.81	1931.93
110	-480.85	1609.64	-468.30	1076.72
140	-378.52	1641.15	-375.19	428.11

A mathematical approximation was used in the shift function (**Figure 28**.). Coefficients C2 from Table 4 are higher values when compared to the difference between rest periods ($C_2 \gg RP - RP_{ref}$). Therefore, the equation in **Figure 28**. reduces to the following equation (Figure 32.). Now, $\frac{C_1}{C_2}$ can be considered as a single coefficient obtained from experimental data.

$$log(\mathrm{a_T}) = \frac{-\mathrm{C_1}}{\mathrm{C_2}}(RP - \mathrm{RP_{ref}})$$

Figure 32. Equation. Approximated shift function for rest period.

The advantage of the above approximation is to reduce the number of variables, as only limited experimental data were available. For any temperature and stress level, $\frac{C_1}{C_2}$ could be computed using Figure 33. . Generally, strains are exponentially related to temperature and hence, exponential interpolation could be used. Linear interpolation was used with respect to stress level. Therefore, linear equations could be used to identify shift coefficient or $\frac{C_1}{C_2}$.

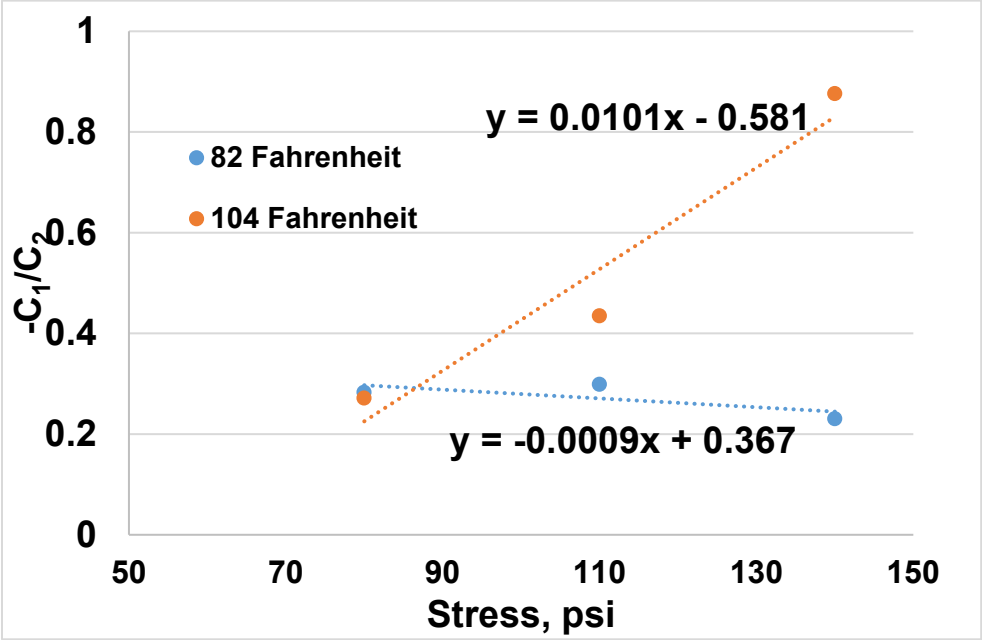

Figure 33. Plot. Shift coefficient versus stress for two temperatures.

Equivalent number of load repetitions (N_{eq}) may be calculated for each sublayer individually. Thus, the effect of rest period could be incorporated into the calculation of rutting for a flexible-pavement system. The procedure is illustrated in the following example.

- Rest period (RP) = 0.52 sec, rest period (RP_{ref}) = 0.18 sec.
- Binder: PG 64-28 SBS
- Temperature: 104°F
- Load level: 140 psi

For variables, $-\frac{C_1}{C_2}$ could be computed to be 0.87 from Figure 33. . Now, a_T could be calculated using Figure 32. .

$$a_T = 10^{\frac{-C_1}{C_2}(RP-RP_{ref})} = 10^{0.87(0.52-0.18)} \approx 2$$

Figure 34. Equation. Calculation of shift factor.

Shift factor implies that the rutting caused over 0.52 sec for load repetition N would be equivalent to rutting caused over 0.18 sec for load repetition $2N$. The phenomenon is presented in Figure 35. . The rutting progression was computed for a thin section (Table 1) with a traffic of 2.500 AADT (only Class 9 vehicles with maximum allowable loads on each axle) at a speed of 40 mph, and it is shown as the orange (reference) curve in Figure 35. . Based on the calculation, an equivalent number of load repetitions for 0.52 sec would be 5,000 AADT of 0.18-sec rest period (two times 2,500 AADT). The blue curve is the progression for a rest period of 0.52 sec at the same 2,500 AADT. Alternatively, 2,500 AADT at a rest period of 0.52 sec is equivalent to 5,000 AADT at 0.18 sec.

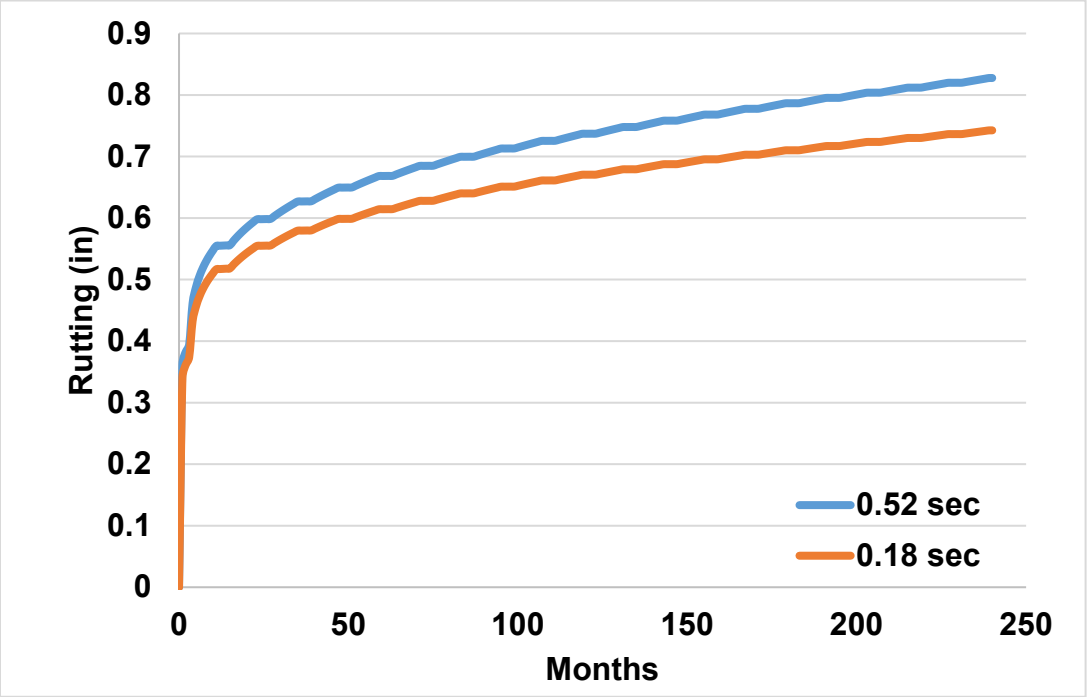

Figure 35. Plot. Rutting progression versus months.

SUMMARY

A model to characterize the effect of rest period on the AC permanent-deformation behavior was introduced. The approach assumes rest period as an additional variable to perform a superposition similar to temperature and time. As rest period increases, rutting increases due to the hardening–relaxation effect. A simplified approach to incorporate the developed shifted-prediction model to the current PMED is introduced.

CHAPTER 5: CONCLUSIONS AND RECOMMENDATIONS

Rest period as a result of spacing of trucks was identified as a key parameter in the optimization of truck platoons. Although reducing truck spacing was shown to reduce aerodynamics resistance and fuel consumption, pavement performance could be negatively impacted. The effects of rest period on the deformation behavior of AC materials were explored using mechanistic and experimental methods. It was confirmed that rest period would be a key variable to consider in optimization of truck platoons with respect to pavement damage. The findings from the mechanistic and experimental tasks are listed below:

- According to the 3-D finite-element analysis using dynamic and moving loads, linear viscoelastic recovery decreases with decreasing spacing between trucks; hence, the rest period resulting in higher total deformations in AC layers.
- A positive effect of decreasing rest period on total and permanent deformations was observed according to the repeated-load permanent-deformation experiments. Permanent deformations substantially reduced with decreasing rest periods, representing the most aggressive truck spacing in platoons.
- The effect of rest period was shown to be a key factor affecting permanent-deformation behavior, with a significance equivalent to stress and temperature levels.
- A shift model was developed by extending the time–temperature superposition concept and framework. The shift model was used to develop equivalent numbers of cycles for loading cases with truck spacings different from a selected reference case. The shift model was proposed as an approach to implement in the current AASHTO PMED.

The following recommendations are made as future research needs:

- Experimental characterization of rest period needs to be extended to stress states better representing truck platoons. The loading cases may include representation of the effect of moving loads and more representative stress states with confinement.
- The shift model needs to be verified with additional experimental data.
- The shift-model implementation needs to be verified with loading examples representing more realistic traffic spectra.

REFERENCES

Alnedawi, A., K. P. Nepal, R. Al-Ameri, and M. Alabdullah (2019). Effect of Vertical Stress Rest Period on Deformation Behaviour of Unbound Granular Materials: Experimental and Numerical Investigations. *Journal of Rock Mechanics and Geotechnical Engineering, 11*(1), 172–180. https://doi.org/10.1016/j.jrmge.2018.05.004.

Al-Qadi, I. L., E. Okte, A. Ramakrishnan, Q. Zhou, and W. Sayeh (2021). *Truck Platooning on Flexible Pavements in Illinois.* Illinois Center for Transportation/Illinois Department of Transportation. FHWA-ICT-21-010.

Al-Qadi, I. L., and P.J Yoo (2007). Effect of Surface Tangential Contact Stresses on Flexible Pavement Response (with Discussion). *Journal of the Association of Asphalt Paving Technologists*, *76*(8), 663–692.

Beranek, Shannon, and Samuel H. Carpenter. 2009. "Fatigue Failure Testing in Section F." *Research Report ICT-09-058*.

Biligiri, K. P., K. E. Kaloush, M. S. Mamlouk, and M. W. Witczak (2007). Rational Modeling of Tertiary Flow for Asphalt Mixtures. *Transportation Research Record: Journal of the Transportation Research Board, 2001*(1), 63–72. https://doi.org/10.3141/2001-08.

Birgisson, B., C. A. Morgan, M. Yarnold, J. Warner, B. Glover, M. P. Steadman, S. Srinivasa, S. Cai, and D. Lee (2020). *Evaluate Potential Impacts, Benefits, Impediments, and Solutions of Automated Trucks and Truck Platooning on Texas Highway Infrastructure Permanent Deformation.* Publication FHWA/TX-21/0-6984-R1. Texas A&M Transportation Institute, The Texas A&M University System, 258.

Carpenter, Samuel H., and Shihui Shen. 2006. "Dissipated Energy Approach to Study Hot-Mix Asphalt Healing in Fatigue." *Transportation Research Record* 1970 (1): 178–185.

Choi, Y.T., and Y. R. Kim (2013). Development of characterisation models for incremental permanent deformation model for asphalt concrete in confined compression. *Road materials and pavement design, 14*(sup2)*,* 266–288.

Darabi, M. K., R. K. A. Al-Rub, E. A. Masad, and D. N. Little (2012). Thermodynamic-based model for coupling temperature-dependent viscoelastic, viscoplastic, and viscodamage constitutive behavior of asphalt mixtures. *International Journal for Numerical and Analytical Methods in Geomechanics, 36*(7), 817–854.

Darabi, M. K., R. K. Abu Al-Rub, E. A. Masad, and D. N. Little (2013). Cyclic Hardening–Relaxation Viscoplasticity Model for Asphalt Concrete Materials. *Journal of Engineering Mechanics, 139*(7), 832–847. https://doi.org/10.1061/(ASCE)EM.1943-7889.0000541.

Daniel, J. S., and Y. R. Kim (2001). Laboratory Evaluation of Fatigue Damage and Healing of Asphalt Mixtures. *Journal of Materials in Civil Engineering, 13*(6), 434–440. https://doi.org/10.1061/(ASCE)0899-1561(2001)13:6(434).

Elseifi, M. A., I. L. Al-Qadi, and P. J. Yoo (2006). Viscoelastic Modeling and Field Validation of Flexible Pavements. *Journal of Engineering Mechanics*, *132*(2), 172–78.

Epps, J. A., National Cooperative Highway Research Program, National Research Council (US), American Association of State Highway and Transportation Officials, and United States, Eds. (2002). *Recommended Performance-Related Specification for Hot-Mix Asphalt Construction: Results of the WesTrack Project.* National Academies Press, Washington, DC.

Fagnant, D. J., and K. Kockelman (2015). Preparing a Nation for Autonomous Vehicles: Opportunities, Barriers and Policy Recommendations. *Transportation Research Part A: Policy and Practice, 77,* 167–181. https://doi.org/10.1016/j.tra.2015.04.003.

Gaudet, Bruce. 2014. "Review of Cooperative Truck Platooning Systems." *National Research Council Canada* 10, 1–79.

Gibson, N. H., C. W. Schwartz, R. A. Schapery, and M. W. Witczak (2003). Viscoelastic, Viscoplastic, and Damage Modeling of Asphalt Concrete in Unconfined Compression. *Transportation Research Record: Journal of the Transportation Research Board, 1860*(1), 3–15. https://doi.org/10.3141/1860-01.

Gungor, O. E., and I. L. Al-Qadi (2020a). All for One: Centralized Optimization of Truck Platoons to Improve Roadway Infrastructure Sustainability. *Transportation Research Part C: Emerging Technologies, 114,* 84–98. https://doi.org/10.1016/j.trc.2020.02.002.

Gungor, O. E., and I. L. Al-Qadi (2020b). Wander 2D: A Flexible Pavement Design Framework for Autonomous and Connected Trucks. *International Journal of Pavement Engineering,* 1–16. https://doi.org/10.1080/10298436.2020.1735636.

Hernandez, J. A., A. Gamez, and I. L. Al-Qadi (2016). Effect of wide-base tires on nationwide flexible pavement systems: Numerical modeling. *Transportation Research Record: Journal of the Transportation Research Board*, *2590*(1), 104–112. https://doi.org/10.3141%2F2590-12

Inc., A., and ERES Division. Appendix GG-1: Calibration of Permanent Deformation Models for Flexible Pavements. NCHRP, 2004.

Jahangiri, B., M. M. Karimi, and N. Tabatabaee (2017). Relaxation of Hardening in Asphalt Concrete under Cyclic Compression Loading*. Journal of Materials in Civil Engineering,* 29(5), 04016288. https://doi.org/10.1061/(ASCE)MT.1943-5533.0001814.

Kim, R., G. Chehab, R. Schapery, M. Witczak, and R. Bonaquist (2003). Characterization of asphalt concrete in uniaxial tension using a viscoelastoplastic continuum damage model. *Journal of the Association of Asphalt Paving Technologists* 72: 315-355.

Kim, Y. R., and D. N. Little. 1989. "Evaluation of Healing in Asphalt Concrete by Means of the Theory of Nonlinear Viscoelasticity." *Transportation Research Record* 1228: 1–13.

Kim, Y. R., S. L. Whitmoyer, and D. N. Little. 1994. "Healing in Asphalt Concrete Pavements: Is It Real?" *Transportation Research Record* 1454: 1–8.

Kim, B., and R. Roque (2006). Evaluation of Healing Property of Asphalt Mixtures. *Transportation Research Record: Journal of the Transportation Research Board, 1970*(1), 84–91. https://doi.org/10.1177/0361198106197000108.

Kim, D., and Y. R. Kim (2017). Development of Stress Sweep Rutting (SSR) Test for Permanent

Deformation Characterization of Asphalt Mixture. *Construction and Building Materials, 154,* 373–383. https://doi.org/10.1016/j.conbuildmat.2017.07.172.

Kim, Y.-R., D. N. Little, and R. L. Lytton (2001). Evaluation of Microdamage, Healing, and Heat Dissipation of Asphalt Mixtures, Using a Dynamic Mechanical Analyzer. *Transportation Research Record: Journal of the Transportation Research Board, 1767*(1), 60–66. https://doi.org/10.3141/1767-08.

Liang, K.-Y., J. Martensson, and K. H. Johansson (2016). Heavy-Duty Vehicle Platoon Formation for Fuel Efficiency. *IEEE Transactions on Intelligent Transportation Systems, 17*(4), 1051–1061. https://doi.org/10.1109/TITS.2015.2492243.

Mallick, Rajib B., and Tahar El-Korchi. "Pavement engineering: principles and practice". *CRC Press*, 2013.

Motevalizadeh, S. M., P. Ayar, S. H. Motevalizadeh, S. Yeganeh, M. Ameri, and K. Bemana. Investigating the Impact of Different Loading Patterns on the Permanent Deformation Behaviour in Hot Mix Asphalt. *Construction and Building Materials, 167*, 707–715. https://doi.org/10.1016/j.conbuildmat.2018.02.049.

National Cooperative Highway Research Program, Transportation Research Board, and National Academies of Sciences, Engineering, and Medicine (2007). *Specification Criteria for Simple Performance Tests for Rutting, Volume I: Dynamic Modulus (E*) and Volume II: Flow Number and Flow Time.* Transportation Research Board, Washington, DC.

Noorvand, H., G. Karnati, and B. S. Underwood (2017). Autonomous Vehicles: Assessment of the Implications of Truck Positioning on Flexible Pavement Performance and Design. *Transportation Research Record: Journal of the Transportation Research Board,* 2640(1), 21–28. https://doi.org/10.3141/2640-03.

Qi, X., and M. W. Witczak (1998). Time-Dependent Permanent Deformation Models for Asphaltic Mixtures. *Transportation Research Record: Journal of the Transportation Research Board, 1639*(1), 83–93. https://doi.org/10.3141/1639-09.

Underwood, B. S., and W. A. Zeiada (2014). Characterization of Microdamage Healing in Asphalt Concrete with a Smeared Continuum Damage Approach. *Transportation Research Record: Journal of the Transportation Research Board, 2447*(1), 126–135. https://doi.org/10.3141/2447-14.

Vavrik, W. R., W. J. Pine, G. A. Huber, S. H. Carpenter, and R. Bailey (2001). The Bailey Method of Gradation Evaluation: The Influence of Aggregate Gradation and Packing Characteristics on Voids in the Mineral Aggregate (with discussion). Journal of the Association of Asphalt Paving Technologists, 70.

Yoo, P., I. L. Al-Qadi, M. Elseifi, and I. Janajreh (2006). Flexible Pavement Responses to Different Loading Amplitudes Considering Layer Interface Condition and Lateral Shear Forces. *The International Journal of Pavement Engineering*, *7*(1), 73–86.

Yoo, P. J., and I. L. Al-Qadi (2007). Effect of transient dynamic loading on flexible pavements. *Transportation Research Record: Journal of the Transportation Review Board*, *1990*(1), 129–140. https://doi.org/10.3141%2F1990-15.

Yun, T. (2008). Development of a Viscoplastic Constitutive Model using Rate-Dependent Yield Criterion for HMA in Compression (Doctoral Dissertation). Retired from https://repository.lib.ncsu.edu/bitstream/handle/1840.16/3103/etd.pdf?isAllowed=y&sequence=1

Yun, T., and Y. R. Kim (2011). A Viscoplastic Constitutive Model for Hot Mix Asphalt in Compression at High Confining Pressure. *Construction and Building Materials, 25*(5), 2733–2740. https://doi.org/10.1016/j.conbuildmat.2010.12.025.

Witzcak, M. W., Ed. (2002). *Simple Performance Test for Superpave Mix Design.* National Academy Press, Washington, DC.

Witzcak, M. W.(2007). Specification Criteria for Simple Performance Tests for Rutting, Volume I: Dynamic Modulus (E*) and Volume II: Flow Number and Flow Time. Transportation Research Board, Washington, D.C., 2007.